Cell Reports
Article

Specificity and Function of Archaeal DNA Replication Initiator Proteins

Rachel Y. Samson,[1,2,6] Yanqun Xu,[3,4,6] Catarina Gadelha,[1,7] Todd A. Stone,[2] Jamal N. Faqiri,[4] Dongfang Li,[5] Nan Qin,[5,8] Fei Pu,[5] Yun Xiang Liang,[3] Qunxin She,[3,4,*] and Stephen D. Bell[1,2,*]

[1]Sir William Dunn School of Pathology, Oxford University, South Parks Road, Oxford OX1 3RE, UK
[2]Molecular and Cellular Biochemistry Department, Department of Biology, Indiana University, Simon Hall, 212 South Hawthorne Drive, Bloomington, IN 47405, USA
[3]State Key Laboratory of Agricultural Microbiology, College of Life Science and Technology, Huazhong Agricultural University, Wuhan 430070, China
[4]Archaeal Centre, Department of Biology, University of Copenhagen, Ole Maaløes Vej 5, DK-2200 Copenhagen N, Denmark
[5]BGI-Shenzhen, Beishan Industrial Zone, Yantian District, Shenzhen 518083, China
[6]These authors contributed equally to this work
[7]Present address: School of Biology, University of Nottingham, Queen's Medical Centre, Nottingham NG7 2UH, UK
[8]Present address: State Key Laboratory for Diagnosis and Treatment of Infectious Disease, The First Affiliated Hospital, Zhejiang University, Hangzhou 310003, PRC
*Correspondence: qunxin@bio.ku.dk (Q.S.), stedbell@indiana.edu (S.D.B.)
http://dx.doi.org/10.1016/j.celrep.2013.01.002

SUMMARY

Chromosomes with multiple DNA replication origins are a hallmark of Eukaryotes and some Archaea. All eukaryal nuclear replication origins are defined by the origin recognition complex (ORC) that recruits the replicative helicase MCM(2-7) via Cdc6 and Cdt1. We find that the three origins in the single chromosome of the archaeon *Sulfolobus islandicus* are specified by distinct initiation factors. While two origins are dependent on archaeal homologs of eukaryal Orc1 and Cdc6, the third origin is instead reliant on an archaeal Cdt1 homolog. We exploit the nonessential nature of the *orc1-1* gene to investigate the role of ATP binding and hydrolysis in initiator function in vivo and in vitro. We find that the ATP-bound form of Orc1-1 is proficient for replication and implicates hydrolysis of ATP in downregulation of origin activity. Finally, we reveal that ATP and DNA binding by Orc1-1 remodels the protein's structure rather than that of the DNA template.

INTRODUCTION

Several archaeal species have multiple origins of replication per chromosome (Lundgren et al., 2004; Norais et al., 2007; Robinson and Bell, 2007; Robinson et al., 2004, 2007). For example, chromosomes of species in the genus *Sulfolobus* are replicated from three origins (Lundgren et al., 2004; Robinson et al., 2004, 2007). All three origins fire once per cell cycle in all cells (Duggin et al., 2008a). Two of the origins, *oriC1* and *oriC2*, lie adjacent to the genes for the candidate initiator proteins Orc1-1 and Orc1-3, respectively (She et al., 2001). Orc1-1 and Orc1-3 share 35% amino acid sequence identity and are related to both eukaryotic Orc1 and Cdc6 (Bell and Dutta, 2002; Robinson and Bell, 2007). There is additionally a third Orc1/Cdc6 protein in *Sulfolobus*, Orc1-2, but it is not encoded adjacent to an origin. The third origin, *oriC3*, lies beside the gene for a crenarchaeal-specific protein, WhiP. WhiP is predicted to have a tandem winged-helix structure reminiscent of bacterial plasmid Rep proteins and has sequence similarity to the eukaryal replication factor Cdt1 (Robinson and Bell, 2007). Biochemical DNA footprinting studies have revealed that complex interactions among the *Sulfolobus solfataricus* Orc1/Cdc6 proteins, WhiP, and the replication origins are possible in vitro (Robinson and Bell, 2007; Robinson et al., 2004, 2007). More specifically, Orc1-1, Orc1-2, and WhiP bind to all three origins, and Orc1-3 binds to *oriC2* and *oriC3*. However, the precise requirements for origin function either in vivo or in vitro remain unknown. The Orc1 proteins are AAA+ proteins that undergo a single-turnover hydrolysis of ATP to ADP, but the functional consequences of ATP binding and hydrolysis are not yet known (Singleton et al., 2004). In the current work, we address these fundamental issues. First, we determine the initiator protein requirements for origin function in vivo in the genetically tractable strain *Sulfolobus islandicus* (Sis) (Guo et al., 2011; Zhang et al., 2010). We find that none of the Orc1/Cdc6 genes are essential for cell viability. Furthermore, we reveal that while *oriC1* requires the *orc1-1* gene product for function, *oriC2* is dependent on Orc1-3. Finally, we find that *oriC3* functions independently of all three Orc1/Cdc6 proteins but requires the Cdt1-related protein WhiP.

Next, we exploit the nonessential nature of Orc1-1 to express mutant forms of the protein and assay their phenotype with respect to *oriC1* firing in vivo. Our data reveal that expression of a Walker B mutant form of the protein that can bind but not hydrolyze ATP leads to an overreplication phenotype, with elevated levels of initiation at *oriC1*. We further observe an enhanced ability of the Walker B mutant protein to recruit MCM to origin DNA in vitro. Finally, we demonstrate that the ATP-bound form of the protein, when bound to DNA, does not

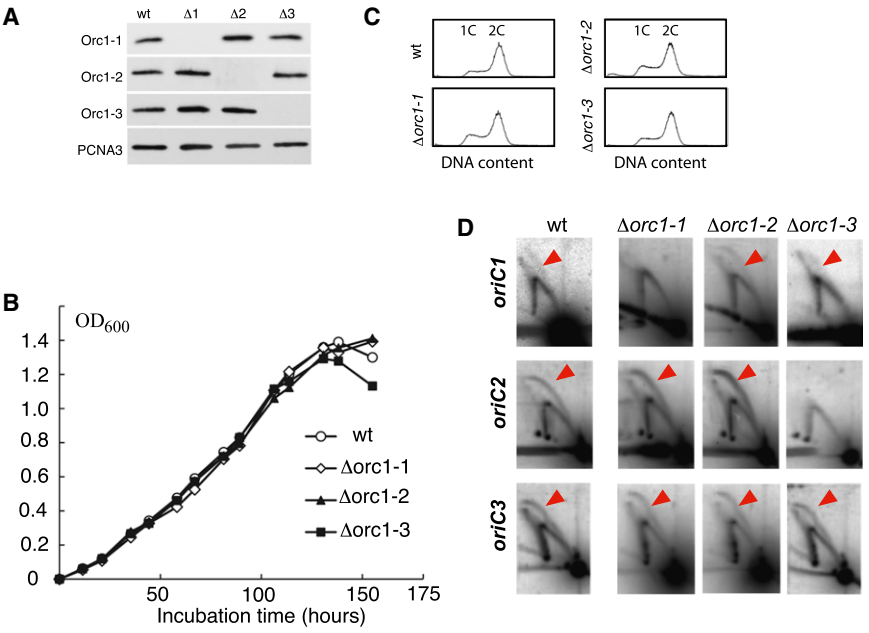

Figure 1. Individual Orc1/Cdc6 Genes Are Nonessential

(A) Western analyses of Orc1/Cdc6 levels in wild-type (wt) and strains deleted for *orc1-1* (Δ1), *orc1-2* (Δ2), or *orc1-3* (Δ3). Antiserum against PCNA3 was used as a loading control.

(B) Growth curves of the indicated strains, following growth by absorbance at 600 nm.

(C) Flow-cytometry profiles of WT and mutant strains. Positions of single- and double-chromosome (1C and 2C) content cells are indicated.

(D) 2D gel analysis of origin activity in wild-type (wt) and the indicated mutant strains. The position of the bubble arc, indicative of replication initiation, is indicated by a red arrowhead.

See also Figures S5, S7, and Tables S1, S2, S3, and S4.

impinge on the geometry of the DNA but remodels its own conformation.

RESULTS

None of the orc1/cdc6 Genes Are Essential for Viability

To address the roles of the individual Orc1/Cdc6 paralogs, we generated mutant *S. islandicus* cell lines in which the relevant genes were deleted (Figure 1A). The resultant strains were viable and showed growth and flow-cytometry profiles that were essentially indistinguishable from the wild-type (WT) strain (Figures 1B and C). We assayed origin activity using two-dimensional (2D) neutral-neutral agarose gel electrophoresis. As can be seen in Figure 1D, deletion of *orc1-1* abrogates firing of *oriC1* but does not affect initiation at *oriC2* or *oriC3*. Deletion of *orc1-2* does not affect firing at any of the three origins, but deletion of *orc1-3* abolishes *oriC2* activity.

Next, we constructed double mutants lacking pairs of Orc1/Cdc6 proteins (Figure 2A). All three possible double mutants were generated, but attempts to generate a triple mutant were unsuccessful. The growth rates of all three double mutants were lower than WT or single mutants, and flow cytometry suggested an elevated S phase population of cells in the Δ*orc1-2*/Δ*orc1-3* and Δ*orc1-1*/Δ*orc1-3* strains (Figures 2B and 2C). The strain lacking both Orc1-2 and Orc1-3 phenocopies the single *orc1-3* deletion, with no firing detectable at *oriC2* but retaining *oriC1* and *oriC3* activity (Figure 2D). Similarly, as observed for deletion of *orc1-1* alone, deletion of both *orc1-1* and *orc1-2* inactivated *oriC1*, but *oriC2* and *oriC3* still fired. (Figure 2D). Significantly, the Δ*orc1-1*/Δ*orc1-3* double mutant only showed replication initiation at *oriC3*; no replication initiation activity was detected at either *oriC1* or *oriC2* in this strain (Figure 2D).

To exclude the possibility that hitherto-undetected cryptic origins might have been activated in the mutant backgrounds, we determined the genome-wide replication profile of the WT and Δ*orc1-1*/Δ*orc1-3* mutant strains by marker frequency analysis (MFA) in conjunction with next-generation sequencing. In agreement with previous studies, three peaks can be observed in the WT strain, corresponding to origin activity at *oriC1*, *oriC2*, and *oriC3* (Figure 2E). As previously seen, the peak at *oriC2* is of lower amplitude due to the broader temporal window of firing of this origin compared to the other two. Significantly, only a single peak is observed in the Δ*orc1-1*/Δ*orc1-3* mutant strain, revealing that the chromosome of this strain is replicated from a single origin, *oriC3* (Figure 2F). There is a modest shoulder on the slope of the peak coincident with the position of *oriC1,* but potential firing here is clearly at a very low level, undetectable by 2D gel analyses and independent of Orc1-1 or Orc1-3. We further note that the trough corresponding to replication termination events is repositioned in this strain to 180° around the chromosome from *oriC3*.

The *whiP* Gene Is Required for *oriC3* Function

Interestingly, none of the individual or double Orc1/Cdc6 gene deletions impinged upon firing of *oriC3*. We therefore speculated that this origin could be functioning independently of Orc1/Cdc6 paralogs. Notably, the Cdt1-related protein WhiP is encoded adjacent to *oriC3* (Robinson and Bell, 2007). Further, we have previously shown that this protein binds to sequence motifs in the *oriC3* region, immediately downstream of the *whiP* gene (Robinson and Bell, 2007). We therefore generated a strain lacking WhiP by introducing tandem stop codons following the start codon of the open reading frame (ORF). The absence of WhiP in the resultant line was confirmed by western blotting (Figure 3A). Cell growth and flow cytometry revealed that the mutant cells grew slower than either WT cells or any of the single *orc1* deletion mutants and with a 2-fold increase in sub-1C signal in the flow cytometry (Figures 3B and 3C). Significantly, loss of the WhiP protein correlated with loss of firing at *oriC3* but had no effect on initiation at *oriC1* and *oriC2*, as adjudged both by 2D neutral-neutral agarose gel electrophoresis analysis and MFA (Figures 3D and 3E). Thus, while *oriC3* is independent of

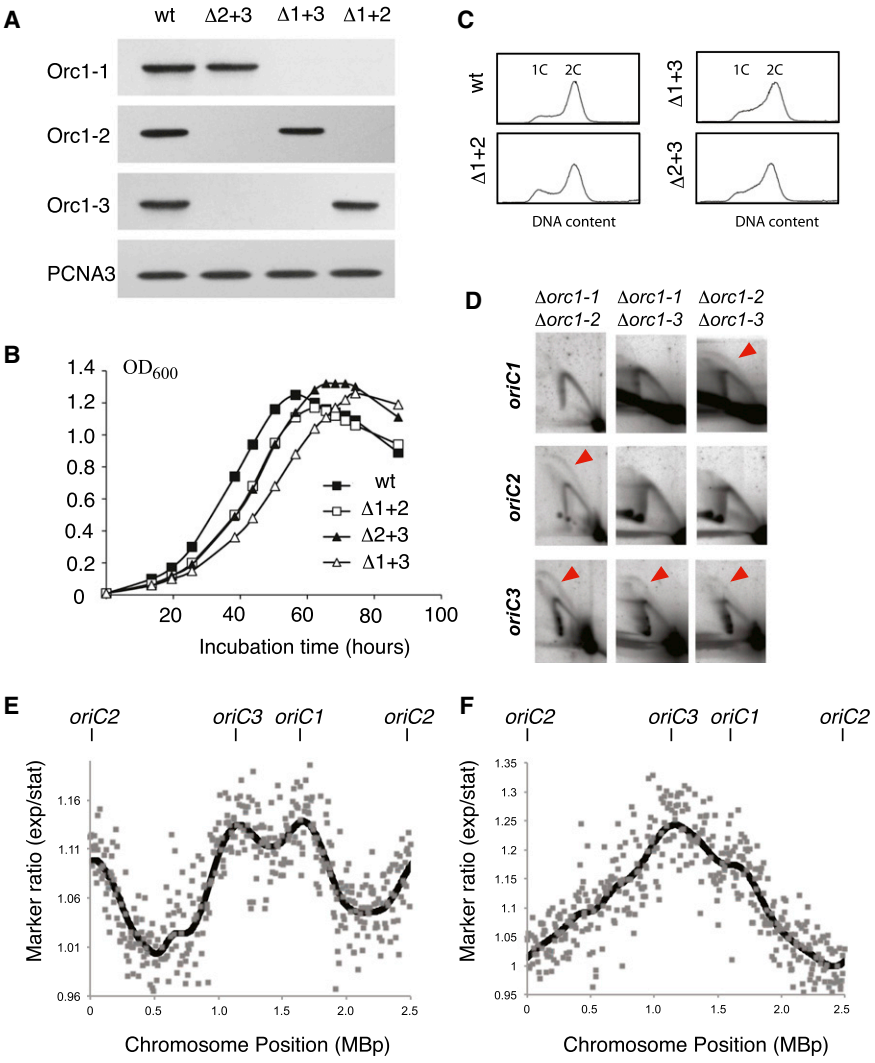

Figure 2. Effect of Deleting Combinations of Orc1/Cdc6 Genes

(A) Western analyses of Orc1/Cdc6 levels in wild-type (wt) and strains deleted for *orc1-2 and orc1-3* (Δ2+3), *orc1-1* and *orc1-3* (Δ1+3), or *orc1-1 and orc1-2* (Δ1+2). Antiserum against PCNA3 was used as a loading control.

(B) Growth curves of the indicated strains, following growth by absorbance at 600 nm.

(C) Flow-cytometry profiles of WT and mutant strains. Positions of single- and double-chromosome (1C and 2C) content cells are indicated.

(D) 2D gel analysis of origin activity in WT (wt) and the indicated mutant strains. The position of the "bubble arc," indicative of replication initiation, is indicated by a red arrowhead.

(E and F) Marker frequency analysis of wild-type cells (E) and cells lacking Orc1-1 and Orc1-3 (F). Marker ratios of sequence tag abundance across the chromosome of exponentially growing cells normalized to nonreplicating stationary phase cells are plotted relative to genome position. The locations of the three origins are indicated above the plots.

See also Figure S7, and Tables S1, S2, S3, and S4.

individual and pairwise combinations of Orc1/Cdc6 proteins (Figures 1 and 2), WhiP is required for replication initiation at this origin (Figures 3D and 3E).

Binding of Initiators to Origins In Vivo

To address origin occupancy by the initiator proteins in vivo, we performed chromatin immunoprecipitation using antisera generated against Orc1-1, Orc1-2, and Orc1-3 and WhiP. In agreement with the lack of requirement for Orc1-2 for firing of any origin, we did not detect binding of Orc1-2 to any of the origins. Also in good agreement with the genetic analyses, we find that *oriC1* is bound by Orc1-1, *oriC2* shows strongest association with Orc1-3, and while no association of any Orc1/Cdc6 protein is observed at *oriC3*, the WhiP protein is specifically localized at this origin (Figures 4A–4D).

Archaea are believed to undergo coupled transcription and translation (French et al., 2007). We were, therefore, concerned that the ability to chromatin immunoprecipitate DNA corresponding to the origins located adjacent to the relevant initiator protein gene could reflect crosslinking of nascent polypeptides to the initiator ORF rather than to the origin itself. We therefore performed chromatin immunoprecipitation sequencing (ChIP-seq) analyses of the three Orc1/Cdc6 proteins and WhiP to give a higher-resolution analysis of the proteins' DNA occupancy. As can be seen in Figures 4E–4G and Figure S1, the relevant proteins showed strong association with the origin loci. Notably, the WhiP ChIP recovers most DNA at internal positions within the WhiP ORF. In addition, a broad but shallow peak was observed over the previously described in vitro binding sites (Robinson and Bell, 2007). These lie at the boundaries of the downstream intergenic region, to which initiation at *oriC3* has been mapped (Robinson et al., 2007). The *whiP* ORF contains conserved AT-rich sequence repeats (Figure S1) and footprinting studies reveal that the protein binds to these with nanomolar affinity. We reiterate that the *whiP* mutation that we employed to inactivate the gene for the genetic studies was by introduction of stop codons at the start of the ORF, rather than by deletion of the ORF (and thus its internal repeats).

In agreement with the 2D gel analyses, we detect Orc1-3 binding at *oriC2* but do not observe significant binding of Orc1-1 to this locus. This was surprising to us because previous ChIP analyses and biochemical and structural studies of the closely related organism, *Sulfolobus solfataricus (*Sso*),* had demonstrated that both Orc1-1 and Orc1-3 bind to *oriC2* in that species (Dueber et al., 2007, 2011; Robinson et al., 2004). However, examination of the sequence of *S. islandicus oriC2* reveals that one of the characterized mini origin recognition

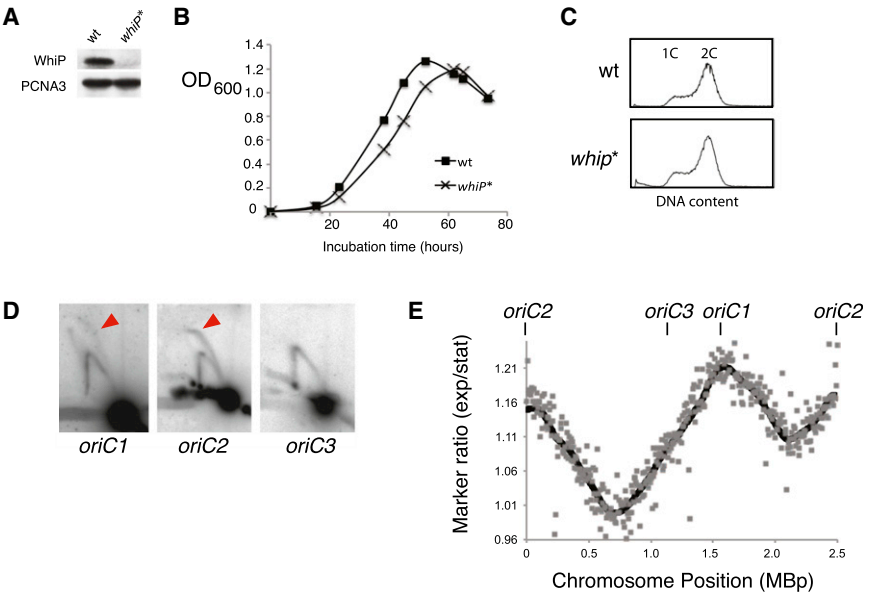

Figure 3. WhiP Mediates Replication Initiation at *oriC3*

(A) Western analyses of WhiP in the wild-type (wt) strain and a strain containing a version of *whiP* with tandem stop codons following the start codon (*whip**).

(B) Growth curves of the indicated strains, following growth by absorbance at 600 nm.

(C) Flow-cytometry profiles of WT and mutant strains. Positions of single- and double-chromosome (1C and 2C) content cells are indicated.

(D) 2D neutral-neutral agarose gels showing *oriC1*, *oriC2*, and *oriC3* activity in the *whip** mutant strain. The position of the bubble arc, indicative of replication initiation, is indicated by a red arrowhead.

(E) MFA profile of the *whip** mutant. The positions of the three origins are shown.

See also Figures S6, S7, and Tables S1, S2, S3, and S4.

box (mORB) Orc1-1 binding sites has several base substitutions in conserved positions in the binding site when compared with *S. solfataricus oriC2* (Figure S2). Additionally, the second mORB element has substitutions immediately adjacent to the core consensus motif. We therefore tested the *S. islandicus* Orc1-1 and Orc1-3 proteins' DNA binding preferences in vitro. Remarkably, but in agreement with the ChIP analyses, Sis Orc1-1 binds with at least 10-fold lower affinity than Sso Orc1-1 to either of the mORB-like elements in Sis *oriC2*. Notably, Sis Orc1-1 has lower affinity for Sso *oriC2* than has Sso Orc1-1. As expected from the ChIP studies, Orc1-3 binds to Sis *oriC2*-derived sequences (Figure S2). Thus, both origin sequence and initiator protein sequence define the differential binding of Orc1-1 to *oriC2* between *S. solfataricus* and *S. islandicus*. Remarkably, even between two closely related species within the *Sulfolobus* genus, we can observe variation within initiator protein specificity and function.

Nucleotide Binding and Orc1-1 Function at *oriC1* In Vivo

We wished to exploit the nonessential nature of Orc1-1 to perform structure-function analyses in living cells. We therefore sought to complement the chromosomal Orc1-1 deletion with a plasmid-encoded copy. Initially, we expressed the gene from its own promoter on a low-copy-number plasmid. We could detect Orc1-1 protein by western blotting (Figure 5A), and the protein localized to *oriC1* as adjudged by ChIP experiments (Figure 6B). However, we were unable to detect any replication initiation at *oriC1* by neutral-neutral 2D agarose gel electrophoresis (Figure 5B). We therefore expressed Orc1-1 from a strong arabinose-inducible promoter (Albers et al., 2006). Either basal or induced expression of the protein from the *araS* promoter led to initiation at *oriC1* as detected by 2D gels (Figure 5B). Indeed, the intensity of the "bubble" arc initiation structure was reproducibly stronger than the rather weak arc observed in WT cells (Figure 5B). This enhanced intensity prompted us to evaluate the DNA content of these cells. Interestingly, cells that express the Orc1-1 protein from the arabinose promoter in either basal or induced conditions show an aberrant flow-cytometry profile with an elevated population of cells, with between 1C and 2C and greater than 2C genome contents (Figure 5C). Furthermore, fluorescence microcopy of these cells reveals altered cell morphologies, with 14% of cells extruding vesicle-like structures (Figure 5D).

Transcription of the *orc1-1* gene in *S. acidocaldarius* and *S. solfataricus* is known to be regulated following perturbation of the cell cycle and after a number of cellular stresses (Fröls et al., 2007; Götz et al., 2007; Lundgren and Bernander, 2007; Ortmann et al., 2008). We therefore wished to determine the profile of expression of this and the other initiator protein genes during a minimally perturbed cell cycle. We employed our previously described "Baby machine" method for synchronizing cells (Duggin et al., 2008a). For these studies, we utilized *S. acidocaldarius* cells because they have given the best synchrony in these experiments. We observe a striking cyclic pattern of transcript levels for *orc1-1*, *orc1-3,* and *whip* (Figure 5E), although we have previously demonstrated that Orc1/Cdc6 protein levels remain constant across the cell cycle (Duggin et al., 2008a). Nevertheless, all three transcripts show lowest levels in S phase and peak in or just before G1 phase. Interestingly, *orc1-3* mRNA levels peak slightly later than *orc1-1*, correlating with the broader temporal window of *oriC2* firing (Duggin et al., 2008a).

The Orc1/Cdc6 proteins possess a AAA+ domain and previous work has shown that this catalyzes a single turnover ATP hydrolysis event, resulting in stable binding of ADP (Singleton et al., 2004). Indeed, Orc1/Cdc6s from a range of archaeal species, when purified as recombinant proteins from bacteria, are isolated exclusively in the ADP-bound form. By analogy with bacterial DnaA, we assumed that the ATP-bound form of Orc1/Cdc6 proteins is the active form (see also below) (Kaguni, 2011; Mott and Berger, 2007). We therefore speculated that the cell-cycle-dependent wave of *orc1-1* transcription

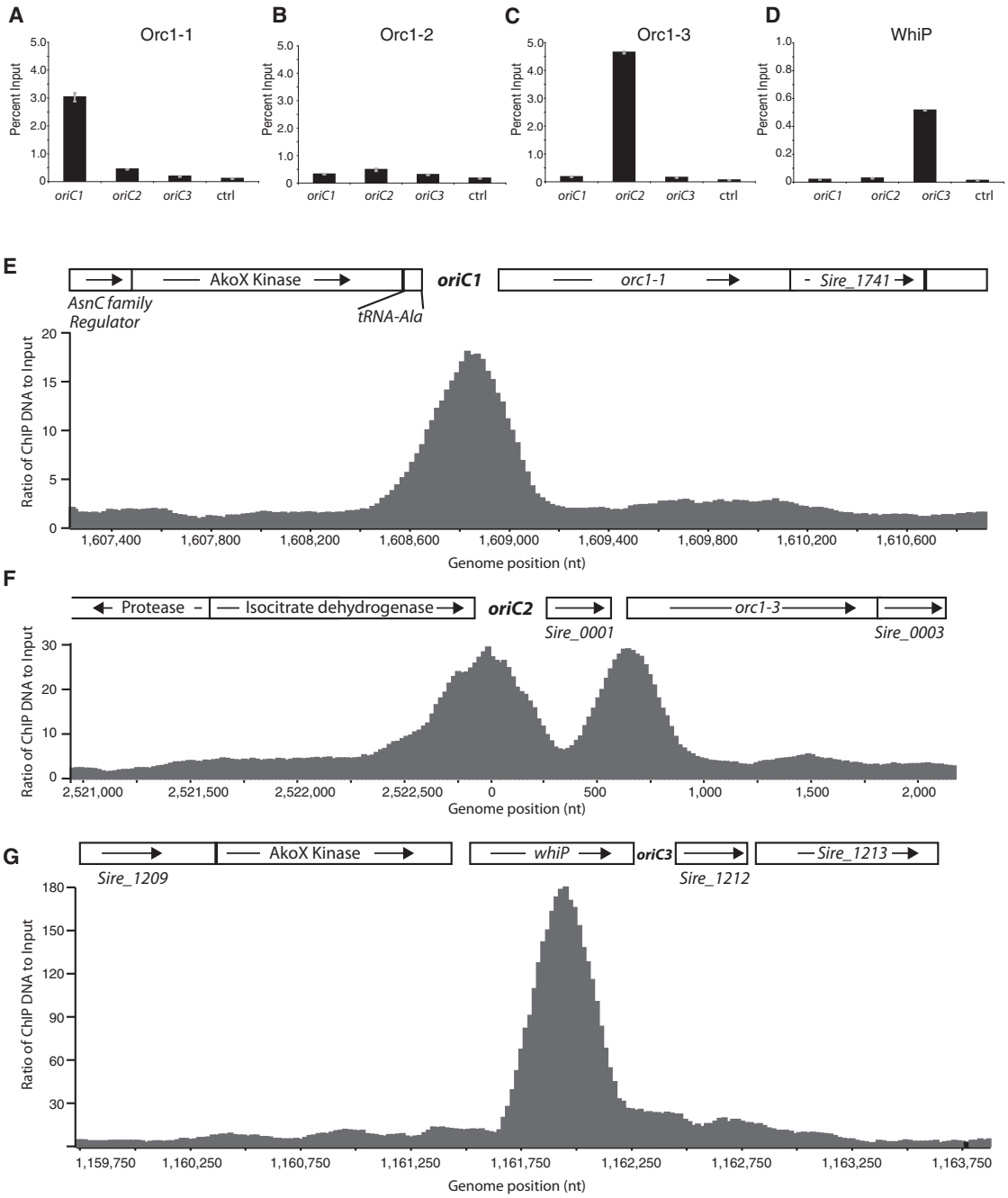

Figure 4. Origin Binding In Vivo by the Orc1/Cdc6 Proteins and WhIP

(A–D) ChIP analyses to assess the binding of the indicated initiator proteins to the three origin loci in vivo. The percent of input DNA recovered was calculated for each origin locus and a distal control locus (ctrl, *SiRe2328*). Bars represent the SD calculated from the triplicate experiments.

(E–G) ChIP-seq results with Orc1-1, Orc1-3, and WhiP antisera, respectively. Genome coordinates are shown below each panel and the location of each origin indicated in bold. See also Figure S1. The y axis scale is the value obtained when normalizing ChIP read counts to input DNA.

See also Figure S2, and Tables S1, S2, S3, and S5.

would result in transiently increased levels of Orc1-1•ATP and that this could create a permissive window for replication initiation. Expressing Orc1-1 constitutively during the cell cycle from the arabinose promoter would result in temporally ectopic Orc1-1•ATP and could thus account for the overreplication phenotype observed. To test this, we created mutant derivatives of Orc1-1 with alterations in the Walker A and Walker B motifs. The Walker A K69A is anticipated to be unable to bind ATP and the Walker B E147A mutant should bind but fail to hydrolyze ATP. These predicted properties were confirmed using purified

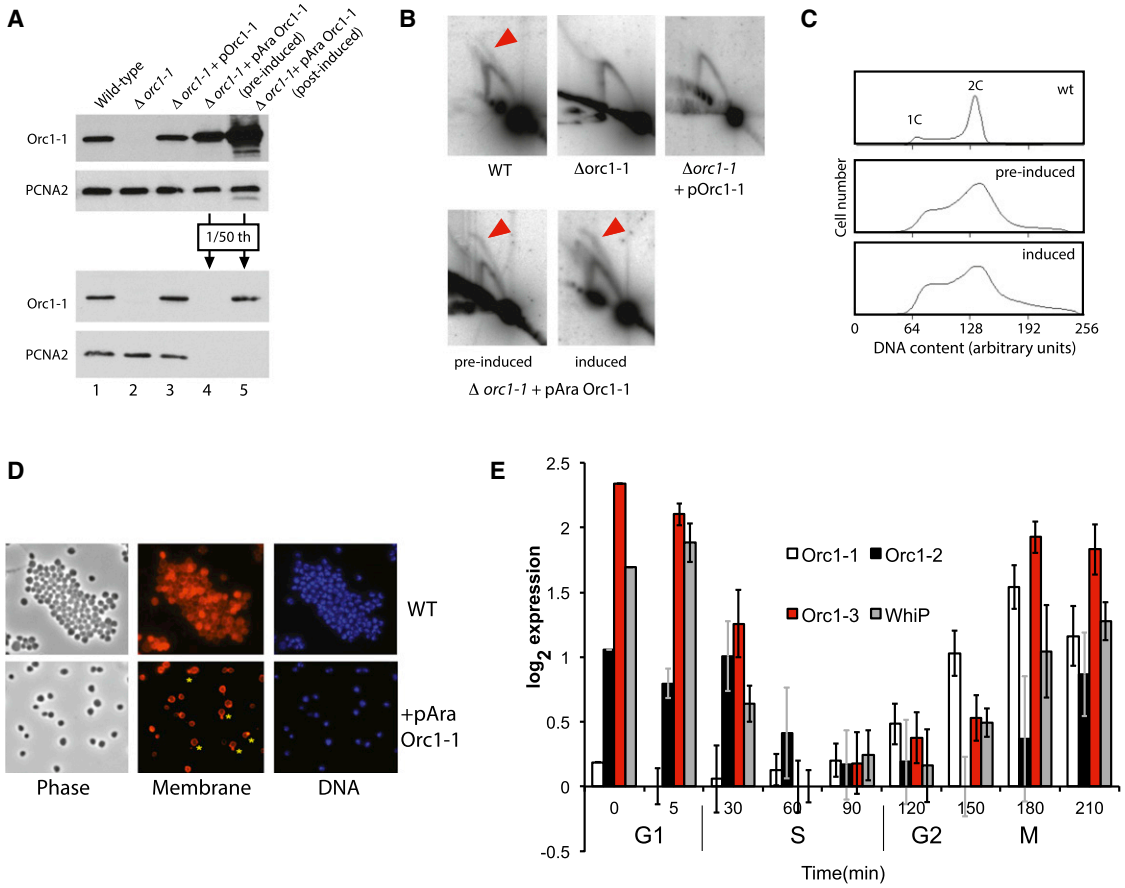

Figure 5. Constitutive Expression of Orc1-1 Causes an Overreplication Phenotype

(A) Western analysis of Orc1-1 levels in WT cells (lane 1), Δ*orc1-1* cells (lane 2), the Δ*orc1-1* strain complemented with a plasmid encoding the gene for Orc1-1 under the control of its native promoter (lane 3), or under the control of the arabinose promoter under noninducing and inducing conditions (lanes 4 and 5). PCNA2 serves as a loading control. Note that in the lower panels the samples in lanes 4 and 5 contain 1/50th the amount of material present in lanes 1–3.

(B) 2D gel analyses of *oriC1* in the indicated strains. The red arrowheads indicate structures arising from replication initiation.

(C) Flow-cytometry analyses of the DNA content of the indicated strains. Peaks corresponding to 1C and 2C cells are indicated.

(D) Micrographs of the indicated strains. Phase contrast, cells stained with the membrane dye FM4-64X (red), and nucleoids stained with DAPI (blue) are shown. Yellow asterisks indicate cells extruding vesicle-like structures.

(E) Transcript abundance profiles of *orc1-1*, *orc1-2*, *orc1-3,* and *whiP* as a function of position in the cell cycle. Cells were synchronized using a baby machine and RNA purified as described (Samson et al., 2011). Bars are ±SD.

See also Figures S3, S4, S7, and Tables S1, S2, and S4.

recombinant proteins (Figure S3). To exclude the possibility of compounding effects due to overexpression, the proteins were then expressed from a plasmid using the native *orc1-1* promoter in the *Δorc1-1* strain (Figure 6A). Despite being expressed and binding to *oriC1* as detected by ChIP, the Walker A mutant failed to support detectable initiation at *oriC1* (Figures 6A–6C). In contrast, the Walker B mutant shows a bubble arc of greater intensity than seen in WT cells (Figure 6C). Furthermore, this strain shows an aberrant flow cytometry profile, with 22% of the population with greater than 2C genome content (Figure 6D). Additionally, microscopy reveals the presence of large cells with elevated DNA content; 13% of Orc1-1 E147A-expressing cells are greater than 1.5 μm in diameter, compared with less than 1% of WT (Figures 6E and 6F). Interestingly, microscopy of the population expressing the Orc1-1 Walker A mutant also shows aberrant large cells (3.8%); however, in agreement with the flow-cytometry profiles, there is not a discernable population of cells with elevated DNA content (as adjudged by DAPI staining). Taken together, our data therefore indicate that the ATP-bound form of Orc1-1 is proficient for origin firing and, furthermore, implicates the hydrolysis of ATP in regulating origin activity.

Biochemical Consequences of ATP Binding by Orc1-1

To investigate the molecular basis of the distinct properties of the proteins, we first performed gel-filtration analyses. These revealed an increase in retention time of the E147A protein compared to WT, suggestive of a conformational alteration (Figure 7A). Next, we performed analytical ultracentrifugation (AUC) with the WT and E147A proteins (Figure 7B; Figure S3). The AUC revealed that the WT protein migrated in two populations, both

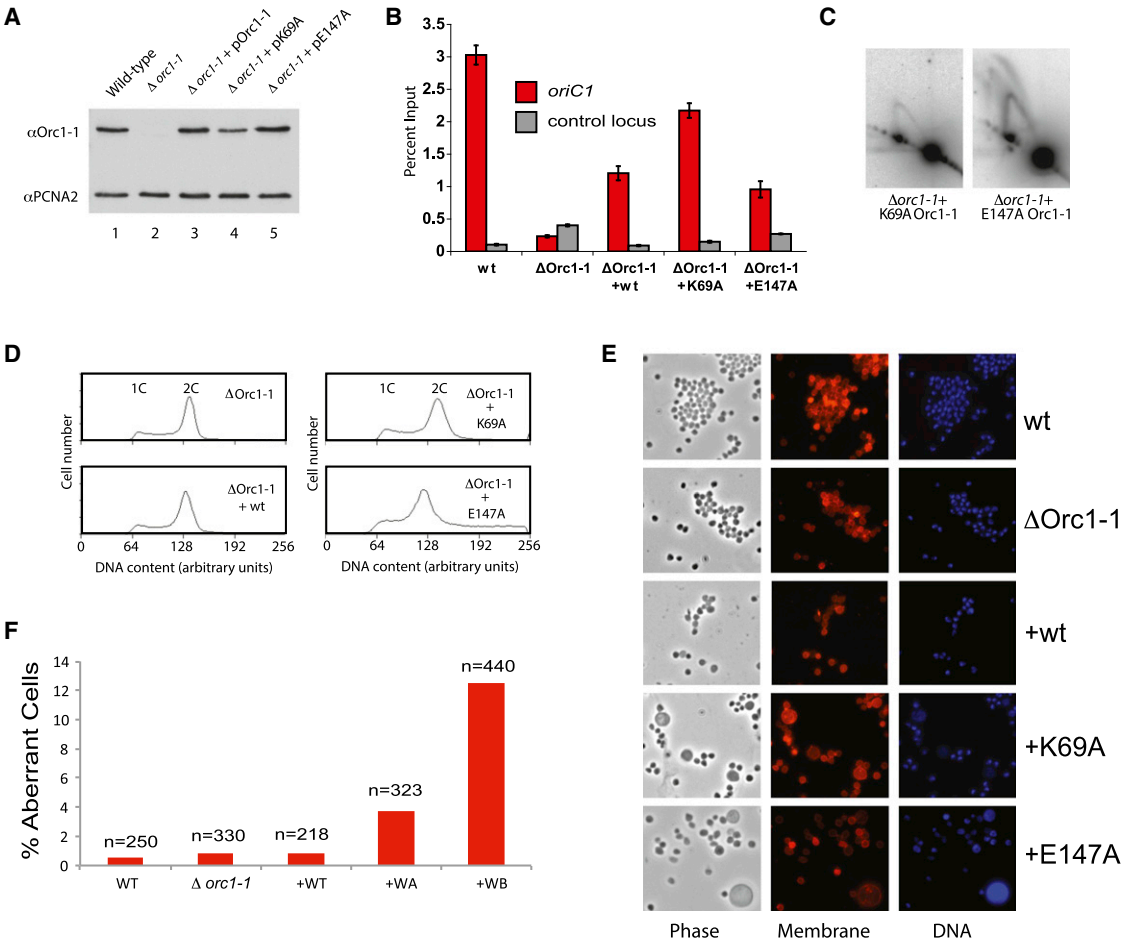

Figure 6. Expression of a Walker B Mutant Orc1-1 Causes an Overreplication Phenotype

(A) Western analysis of Orc1-1 levels in WT (lane 1) and Δorc1-1 (lane 2) strains and the latter strain complemented with a plasmid encoding the gene for WT Orc1-1 (lane 3), K69A Walker A mutant (lane 4), and E147A Walker B mutant (lane 5) under the control of the native *orc1-1* promoter.

(B) ChIP analysis of the indicated Orc1-1 protein binding to *oriC1* and a distal control locus (*Sire_2328*) in vivo. Error bars are ±SD.

(C) 2D gel analyses of replication initiation at *oriC1* in the indicated strains. Red arrowheads indicate structures arising due to replication initiation.

(D) Flow-cytometry analyses of the cell-cycle profile of the indicated strains. Positions of 1C and 2C populations are indicated.

(E) Micrographs of the indicated strains (+wt = Δorc1-1 + pOrc1-1, +K69A = Δorc1-1 + pOrc1-1 [K69A]; +E147A = Δorc1-1 + pOrc1-1 [E147A]). Phase contrast, membrane dye FM4-64X (red), and DAPI-stained (blue) images are shown.

(F) Quantitation of aberrant cells (scored as having a diameter greater than 1.5 μm). Note that large cells in the Walker A strain appear to have less DNA than the large cells in the Walker B strain.

See also Figures S3, S4, S7, and Tables S1, S2, and S4.

corresponding to monomer with distinct conformations. More specifically, 8.3% of the population had a sedimentation coefficient of 2.8 s and frictional ratio of 1.37, revealing a more extended configuration than the majority of the protein that resolved in a peak at 3.7 s with a frictional ratio of 1.07 and thus was more globular. Interestingly, very different behavior was observed with E147A. Although 65% of the E147A protein behaved as globular monomer (frictional ratio of 1.03), there was no peak corresponding to the extended monomer configuration. However, E147A generated a peak with a mass compatible with the formation of a dimer. Furthermore, the sedimentation coefficient and frictional ratio of the monomeric form of the E147A protein were lower than those of the majority WT species, indicating that it adopted a distinct conformation.

Structural studies have revealed that the ADP-bound forms of Orc1/Cdc6 proteins make bidentate interactions with DNA, binding via the C-terminal wH domain and the initiator-specific motif (ISM) in the AAA+ domain. To date, there is no structure available of the ATP-bound form of Orc1/Cdc6 on DNA. However, Wigley and colleagues were successful in denaturing Orc1-2 from *Aeropyrum pernix* (Ape), removing ADP and refolding in the presence of the nonhydrolyzable ATP analog, ADP-NP, prior to crystallization and structure determination (Singleton et al., 2004). The resultant structure revealed a significant alteration in the relative positioning of the wH and AAA+ domain compared to the various conformations adopted by the ADP-bound form (Singleton et al., 2004). Ape Orc1-2 has only 22% sequence identity to *S. islandicus* Orc1-1 and belongs to

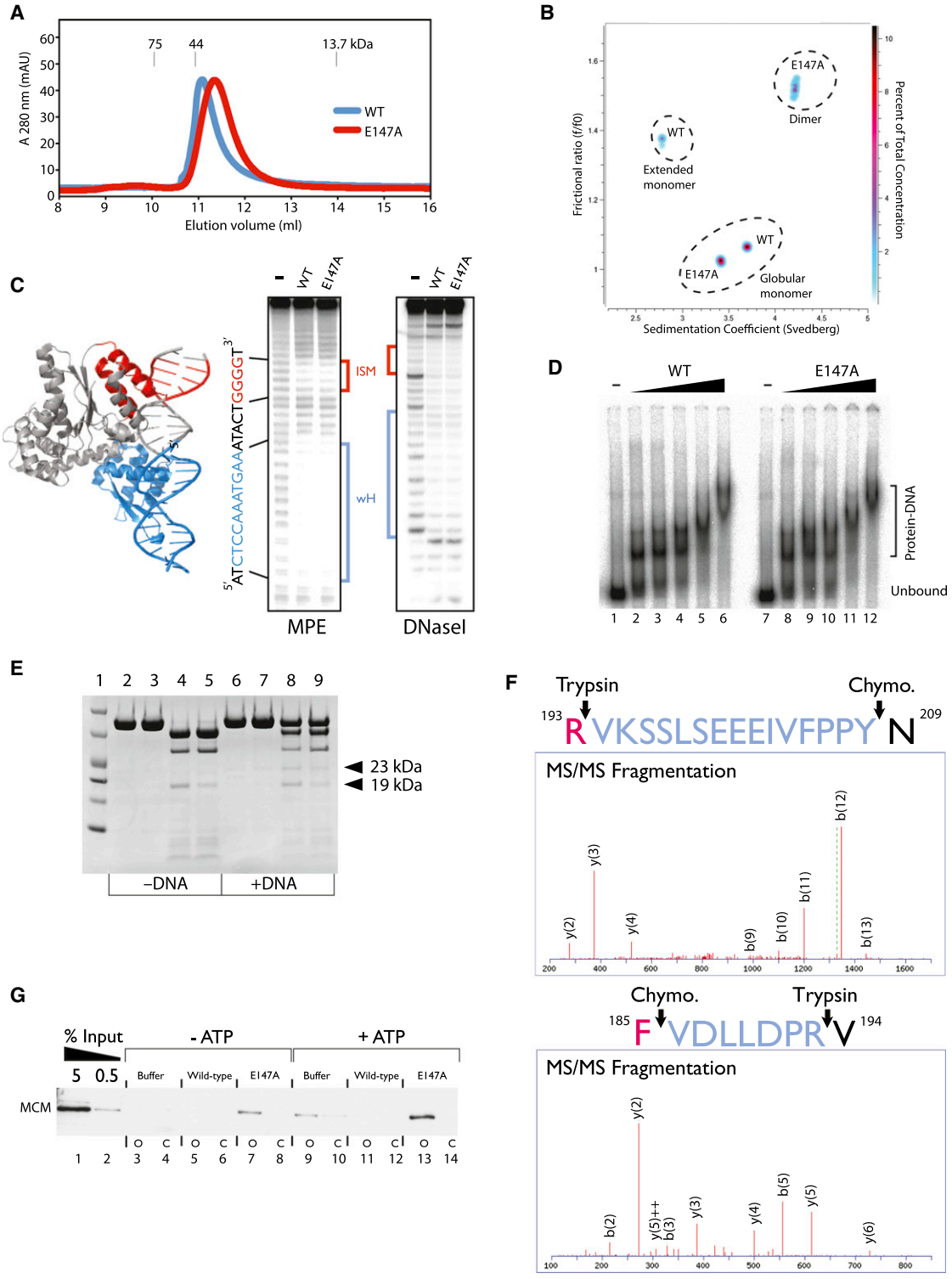

Figure 7. Biochemical Consequences of the Walker B E147A Mutation

(A) Nucleotide-dependent conformational changes in Orc1-1. Gel filtration analysis of 10 μg of WT Orc1-1•ADP or the E147A•ATP on a Superdex 75 column. The elution positions of size standards are indicated (conalbumin, 75 kDa; ovalbumin, 44 kDa; and ribonuclease A, 13.7 kDa).

(B) Composite three-dimensional contour plot of hydrodynamic parameters obtained from GA-MC50 analysis of WT and Walker B mutant Orc1-1 (E147A). WT analysis reveals the presence of two conformers of the monomer, while the Walker B mutant results indicate the presence of a single monomer conformer in addition to a dimer form (see also Figure S3).

(legend continued on next page)

a distinct clade of Orc1/Cdc6s; nevertheless, our AUC and gel filtration data suggest that the identity of the nucleotide bound by Orc1-1 also modulates the conformation of this protein in solution.

Superimposition of the ADP-NP-bound Orc1-2 structure onto the Orc1-1•ADP–DNA structure, aligning via the principal DNA-binding wH domain, suggests three possible consequences of ATP binding (Figure S4). First, the ISM could disengage from the DNA, conceivably allowing the AAA+ domain to be accessible for interaction with another protomer or client protein; second, both wH and ISM could remain engaged with DNA with consequent remodeling of the intervening duplex DNA; third, both domains remain engaged with DNA and the protein undergoes an internal conformational alteration without modulating DNA structure. To test for the first two scenarios, we performed methidium propyl EDTA footprinting with the WT and E147A proteins on an isolated DNA binding site, the ORB2 element. This technique allows clear resolution of the DNA sequences contacted by wH and ISM. As can be seen from Figure 7C, no discernable difference is seen between the protection patterns mediated by the two proteins, indicating no significant disengagement from, or remodeling of, the DNA binding site. Similarly, there was no discernable difference in the protection pattern upon DNaseI digestion. The same result was observed with ORB1 and ORB3 DNA (data not shown). Furthermore, electrophoretic mobility shift assay (EMSA) analysis with full-length origin DNA fragments (Figure 7D) reveals no significant changes in the affinity for DNA or pattern of shifted complexes generated by either the Orc1-1•ADP or the Orc1-1 E147A•ATP forms of the protein. Additionally, we could not detect melting of origin DNA, by either potassium permanganate or nuclease P1 sensitivity, by either protein in the presence or absence of nucleotide (data not shown). In light of our AUC and gel filtration data revealing altered conformations of the monomeric protein, we therefore speculated that the principal effect of ATP binding was on the conformation of the protein itself rather than on that of the DNA. To investigate this further, we subjected WT and Walker B mutant Orc1-1 to limited proteolysis with trypsin in the presence and absence of saturating levels of ORB2 DNA. Under both conditions, we observe reduced levels of a ~19 kDa species with the Walker B mutant form. In the presence of DNA, the digest patterns of both forms of the protein are altered, with a novel 23 kDa species appearing (Figure 7E). This species was also more abundant with the WT protein. We recovered the gel bands, digested them with chymotrypsin, and subjected the resultant peptides to mass spectrometry (Figure 7F). The upper band yielded two peptides that corresponded to the product of trypsin digestion at R193 and chymotrypsin digestion at Y208 or F185. This is in good agreement with the apparent size of the species of ~23 kDa (trypsin cleavage at R193 would generate a C-terminal fragment of 22.8 kDa and a N-terminal fragment of 22.5 kDa). The ~19 kDa band also yielded a peptide derived from trypsin cleavage at R193 and chymotrypsin at F185. Thus, the ATP-bound form of Orc1-1, both in DNA-bound and unbound form, displays altered sensitivity of R193 to trypsin digestion. Significantly, R193 corresponds to the arginine finger of the protein's AAA+ site. Thus, in the absence of any observable alterations to the affinity, geometry, or stoichiometry of the protein-DNA interaction between Orc1-1 and DNA, we propose that the differential sensitivity to trypsin reflects a conformational alteration of the ATP-bound form of the protein on DNA that renders it permissive to recruitment of the MCM helicase.

Finally, we established an in vitro assay for MCM recruitment to *oriC1*. In this assay, we immobilized origin or nonorigin DNA on paramagnetic beads, preincubated with WT (ADP-bound) or E147A Orc1-1 in the presence or absence of supplemental ATP and then added cell extract prepared from logarithmically growing *S. islandicus* cells. Following incubation at 50°C and washing, beads were recovered and bound proteins eluted by boiling in SDS-PAGE loading buffer prior to western blotting. As can be seen in Figure 7G, neither extract alone nor extract supplemented with WT (ADP-bound) Orc1-1 supports significant MCM recruitment in the absence of ATP. Extract with additional ATP supports recruitment, but interestingly this recruitment is lost by the addition of 1 μM WT Orc1-1•ADP, presumably as a consequence of competition with endogenous Orc1-1 for the 200 pM template. Importantly, however, the E147A mutant supported robust, ATP-stimulated recruitment of MCM in these assays.

DISCUSSION

Taken together, our data yield insight into the evolution, regulation, and mechanism of replication initiation in the chromosome of *Sulfolobus* species. We find that the chromosome is a mosaic

(C) The structure of the *Aeropyrum pernix* Orc1-1 ortholog bound to an ORB element from *oriC1* is shown. The ISM is shown in red and the wH domain in blue. (Figure generated using Pymol from Protein Data Bank file 2V1U.) DNA contact points are correspondingly color-coded. The structure is aligned to the sequence of the *S. islandicus oriC1* ORB2 element. The left-hand gel image shows Fe•MPE cleavage patterns in the absence (−) or presence of 1 μM WT or Walker B E147A mutant protein (WB) in the presence of 2 mM ATP (WB). Positions of protection from cleavage are identified at the right of the panel. The right-hand panel shows DNaseI footprinting performed in the absence (−) or presence of 1 μM WT or Walker B E147A mutant protein (WB) in the presence of 2 mM ATP (WB).

(D) EMSA analysis of WT or Walker B E147A mutant protein binding to a 231 nt probe containing *S. islandicus oriC1*. Lanes contain 0, 63, 125, 250, 500, or 1000 nM of the indicated Orc1-1 protein.

(E) Trypsin cleavage products following 22 hr digestion of WT (lanes 2, 4, 6, and 8) and Walker B mutant (lanes 3, 5, 7, and 9) in the absence (lanes 2–5) or presence (lanes 6–9) of ORB2 DNA.

(F) Identity of the terminal trypsin digestion site by determined by liquid-chromatography tandem mass spectrometry.

(G) Western analysis of MCM recruitment to paramagnetic beads containing either control DNA (c) or *oriC1*-containing DNA (o). Reactions contained DNA at 200 pM and were preincubated with buffer (lanes 3, 4, 9, and 10) or 1 μM WT recombinant protein (lanes 5, 6, 11, and 12) or Walker B mutant E147A Orc1-1 (lanes 7, 8, 13, and 14) in the presence (lanes 9–14) or absence (lanes 3–8) of 2 mM ATP. Following preincubation, extract was added, incubated, and then washed prior to elution of bound proteins by boiling with SDS PAGE loading buffer. 5 and 0.5% input extract were loaded in lanes 1 and 2. MCM was detected by western blotting. See also Figure S4.

of three distinct replicons, each with its own principal initiator protein. In particular, we note that initiation at *oriC3* is not impacted upon by individual or combined Orc1/Cdc6 deletions but is abrogated by loss of expression of the Cdt1 homolog WhiP. Intriguingly, parallels can be drawn with metazoa: in *Drosophila*, the origin recognition complex (ORC) is dispensable for endoreduplication, whereas Cdt1 is essential for this process (Park and Asano, 2008). We note that it was not possible for us to generate a triple Orc-1 mutation in which all three paralogs were deleted. Given that Orc1-2 does not bind in vivo to any origin, we speculate that this synthetic lethality may reflect nonorigin roles for the Orc1/Cdc6 proteins. Indeed, our ChIP-seq analyses reveal multiple nonorigin genomic binding sites for the Orc1/Cdc6 proteins. Furthermore, the single mutants show significantly altered transcript profiles compared to WT cells (R.Y.S. and S.D.B., unpublished data). Thus, as with DnaA and eukaryal ORC proteins (Scholefield et al., 2011), it appears that archaeal Orc1/Cdc6 proteins play roles in transcriptional regulation.

We speculate that the mosaic nature of the *Sulfolobus* chromosome has arisen by integration of extrachromosomal elements into an ancestral chromosome that presumably contained a single origin of replication. Given the broad conservation of Orc1-1 orthologs and their DNA binding sites across the archaeal domain of life (Robinson et al., 2004), we suggest that the ancestral chromosome was dependent on Orc1-1 and *oriC1*. Because WhiP homologs are found in the *Desulfurococcales* and *Sulfolobales* and Orc1-3 is restricted to the *Sulfolobales*, we propose the sequential acquisition of first WhiP/*oriC3* prior to the bifurcation of these two lineages, followed by integration of the Orc1-3/*oriC2* replicon in the branch leading to the *Sulfolobales*. Interestingly, the genome replication mode of the bacterium *Vibrio cholera* also appears to have been sculpted by acquisition of extrachromosomal element replication origins. However, in that organism, the genome is split between two chromosomes, each with a single origin: one dependent on a classic bacterial *oriC*/DnaA system and the second having an origin with features reminiscent of plasmid origins. Indeed, this partitioning of bacterial genomes into multiple single-origin chromosomes is found in a range of bacterial species (Egan et al., 2005; Egan and Waldor, 2003). In contrast, multiple-origin single-chromosome genomes are found in a number of archaea. Why are archaeal chromosomes permissive in this regard? One explanation may lie in the contrasting mechanisms for replication termination in bacteria versus archaea (Duggin et al., 2008b; Toro and Shapiro, 2010). Whereas termination in bacteria involves polar fork traps, we have recently found that termination in *Sulfolobus* is by random fork collision (Duggin et al., 2011). In support of this, our MFA data on the mutant strains in which only a single origin fires reveal that termination is repositioned to occur 180° across the chromosome from the active origin (Figure 2F). An ectopic origin integrated into one replichore of a bacterial chromosome would result in premature arrival and prolonged stalling of a fork at a termination site. This may impact genome stability. In addition, because of the presence of the fork traps, the time taken to replicate a two-origin bacterial chromosome would still be dependent on the length of time it takes the fork arising from *oriC* to traverse the longest replichore. In contrast, the absence of active termination sites in *Sulfolobus* would mean that additional origins would simply result in repositioning of termination events to midway between active origins and a concomitant reduction in the total time spent in S phase, assuming similar timing of firing of the origins. The ability to accommodate and regulate multiple origins will have played a major role in permitting the increase in genome size seen in eukaryotic organisms (Diffley, 2011).

Our data also reveal mechanistic insight into the action of the Orc1-1 initiator. As with bacterial DnaA, we find that the ATP-bound form of the initiator is the active form (Kaguni, 2011; Mott and Berger, 2007). Our expression profiling reveals a wave of transcription of the genes for the Orc1-1 and Orc1-3 initiators immediately prior to the onset of replication. We propose that this imposes a temporal window for initiation in which the newly synthesized proteins bind to ATP and associates with origin DNA before hydrolysis of ATP to ADP inactivates the proteins. It may, therefore, be significant that Orc1-1 and Orc1-3 are encoded in the immediate vicinity of their cognate origins. Furthermore, expression of WT Orc1-1 driven by its native promoter from episomes, while resulting in origin occupancy (as adjudged by ChIP), fails to activate the origin, presumably due to hydrolysis of ATP in the cell prior to origin binding. However, expression of the Walker B ATP hydrolysis-defective mutant to the same level results in an overreplication phenotype.

In bacteria, the ATP-bound form of DnaA facilitates the formation of higher-order structures and is able to mediate localized DNA melting at the origin (Bramhill and Kornberg, 1988; Duderstadt et al., 2011; Erzberger et al., 2006; Katayama et al., 2010; Ozaki et al., 2008). Although we do observe a subpopulation of the Walker B mutant form of the protein existing as dimer in solution, we find that the ADP- and ATP-bound forms of Orc1-1 show equivalent DNA binding properties. Furthermore, we have been unable to observe any localized sensitivity to nuclease P1 or potassium permanganate, indicative of DNA melting, induced by either form of the protein (data not shown). Perhaps unsurprisingly, in this regard Orc1-1 is behaving in a manner more reminiscent of eukaryal ORC. There is no evidence for eukaryal ORC melting origins; rather, the available data support a model whereby MCM(2-7) is recruited to double-stranded DNA with duplex unwinding occurring at a later stage (Evrin et al., 2009; Heller et al., 2011; Remus et al., 2009). We propose that this is an evolutionarily conserved feature of the Orc1/Cdc6 proteins and that these proteins act principally to define loci for MCM recruitment. In light of our protease sensitivity assays, we suggest that ATP acts to modulate the conformation of Orc1/Cdc6 proteins on the DNA binding site such that the protein is able to effectively recruit MCM. Subsequent hydrolysis of ATP to ADP by Orc1/Cdc6 then renders the protein incapable of recruiting further MCM, thereby contributing to the fidelity of replication control. This simple binary switch model of archaeal Orc1/Cdc6 function is supported by our observation of the overreplication phenotype mediated by the Walker B mutant of Orc1-1. We note that in budding yeast, temporally distinct ATP binding and hydrolysis events by both the ORC complex and Cdc6 are required for iterative MCM(2-7) loading at replication origins (Randell et al., 2006). The increased organizational complexity of the eukaryotic origin definition and MCM recruitment system is likely a consequence of the increased regulatory demands

imposed by the large number of replication origins found in eukaryotic chromosomes (Diffley, 2011). The simple binary-switch model that we propose for Orc1/Cdc6 function is clearly distinct from the mechanism of action of the bacterial initiator DnaA and provides a paradigm for the function of initiator proteins in archaea and eukaryotes.

EXPERIMENTAL PROCEDURES

Strains, Media, and Growth Conditions

S. islandicus strain E233S (Δ*pyrEF* Δ*lacS*) constructed previously (Deng et al., 2009) was used as the host for genetic manipulations. All archaeal strains used in this work, including the genetic host and its transformants of diverse plasmids as well as the *orc1/whip,* are summarized in Table S1. These archaeal cell lines were grown in SCVY (0.2% sucrose, 0.2% Casamino acids, 5 ml vitamin solution, and 0.005% yeast extracts) or TYS (0.1% tryptone, 0.05% yeast extracts, and 0.2% sucrose) medium at 78°C. If required, uracil was supplemented to 20 μg/ml while 5′-fluoorooritic acid (5′-FOA) was added to 50 μg/ml, in SCVY medium. Microscopy was performed as described previously (Samson et al., 2011).

Protein Purification and Biochemical Analyses

Orc1/Cdc6 and WhiP proteins were expressed in *E. coli* with C-terminal Hexa-His tags and purified as described previously (Robinson and Bell, 2007; Dueber et al., 2007). EMSAs and footprinting were performed as described previously (Dueber et al., 2007; Robinson et al., 2004). The MCM recruitment assay was based on the approach initially established by Seki and Diffley (2000). A total of 10 μg of a 5 kb plasmid (pCR Script containing a 2 kb sequence centered around *oriC1* or a control locus, *Sire_2328*) was linearized by EcoRI and PstI digestion, the EcoRI-generated recessed end was filled in with Klenow fragment (New England Biolabs) and Biotin-14-dATP and dTTP. The DNA was recovered from the reaction mixture using QiaQuick column (QIAGEN) and immobilized on Dynabeads M-280 streptavidin beads following the manufacturer's recommendations (Life Technologies). Binding reactions were assembled in LoBind tubes (Eppendorf) and contained 200 pM DNA in 50 μl of binding buffer (20 mM Tris acetate, 50 mM potassium acetate, 10 mM magnesium acetate, 1 mM DTT [pH 7.9] at 25°C) plus 20 ng/μl poly(dGdC). Reactions were heated to 50°C in a water bath and buffer or Orc1-1 protein (1 μM final) were added and supplemented with nucleotide to 2 mM as indicated. Following a 10 min incubation, 20 μl of a 5 mg/ml whole-cell extract of *S. islandicus* was added (see below). Then, 20 μl of water or supplemental ATP to 2mM as indicated was added and the reaction incubated for a further 30 min at 50°C before washing twice by magnet-mediated bead pelleting and resuspension in 100 μl of prewarmed binding buffer, followed by one wash in 100 μl binding buffer containing 500 mM potassium acetate. Following this final wash, beads were resuspended in 1xSDS PAGE loading buffer and subjected to SDS PAGE followed by western blotting. All wash steps employed preheated buffers and were performed in the 50°C water bath. We observed a very high background of recombinant Orc1-1 protein bound to both DNA substrates and even to beads alone (data not shown), but MCM was only efficiently recruited to the origin-containing DNA substrate.

The *S. islandicus* cell extract was prepared by growing cells to midexponential phase (OD 600 nm = 0.4) before harvesting and resuspension in 2x binding buffer (40 mM Tris acetate, 100 mM potassium acetate, 20 mM magnesium acetate, 2 mM DTT [pH 7.9] at 25°C). Cells were lysed using a FrenchPress (Thermo) and the extract was clarified by centrifugation at 23,700 *g* for 15 min at 4°C. Then, 100 μl aliquots were prepared in LoBind tubes and snap frozen on dry ice. Total protein concentration was determined by Bradford assay to be 5 mg/ml. Extracts were stored at −80°C.

Flow Cytometry

Flow cytometry of *S. islandicus* cells was performed essentially as previously described for *S. acidocaldarius* (Duggin et al., 2008a). Cells were fixed with 70% ethanol and their DNAs were stained with Mithramycin A and analyzed with A-40 Apogee flow cytometer.

Neutral-Neutral 2D Gel Electrophoresis

S. islandicus cells were collected by centrifugation and washed twice with TEN buffer (50 mM Tris-Cl [pH 8], 50 mM EDTA [pH 8], 100 mM NaCl). Cell suspensions were then mixed with low-melting-point agarose and dispensed into Bio-Rad plug molds. Genomic DNA preparation and 2D gel electrophoresis were performed as described previously (Robinson et al., 2004). For further details, please refer to Extended Experimental Procedures.

Chromatin Immunoprecipitation

ChIP was performed as described by Robinson et al. (2004). For further details, please refer to Extended Experimental Procedures.

SUPPLEMENTAL INFORMATION

Supplemental Information includes Extended Experimental Procedures, seven figures, and five tables and can be found with this article online at http://dx.doi.org/10.1016/j.celrep.2013.01.002.

LICENSING INFORMATION

ACKNOWLEDGMENTS

Work in Q.S.'s laboratory is supported by a special grant from Huazhong Agricultural University and the Danish Independent Research Councils (FTP/11-106683), and work in S.D.B.'s laboratory is funded by the Wellcome Trust (086045/Z/08/Z) and by the College of Arts and Sciences, Indiana University. We thank the staff at the Wellcome Trust Center for Human Genetics for performing the NGS described in Figure 3E.

Received: May 2, 2012
Revised: October 9, 2012
Accepted: January 3, 2013
Published: January 31, 2013

REFERENCES

Albers, S.V., Jonuscheit, M., Dinkelaker, S., Urich, T., Kletzin, A., Tampé, R., Driessen, A.J.M., and Schleper, C. (2006). Production of recombinant and tagged proteins in the hyperthermophilic archaeon Sulfolobus solfataricus. Appl. Environ. Microbiol. *72*, 102–111.

Bell, S.P., and Dutta, A. (2002). DNA replication in eukaryotic cells. Annu. Rev. Biochem. *71*, 333–374.

Bramhill, D., and Kornberg, A. (1988). Duplex opening by dnaA protein at novel sequences in initiation of replication at the origin of the E. coli chromosome. Cell *52*, 743–755.

Deng, L., Zhu, H., Chen, Z., Liang, Y.X., and She, Q. (2009). Unmarked gene deletion and host-vector system for the hyperthermophilic crenarchaeon Sulfolobus islandicus. Extremophiles *13*, 735–746.

Diffley, J.F.X. (2011). Quality control in the initiation of eukaryotic DNA replication. Philos. Trans. R. Soc. Lond. B Biol. Sci. *366*, 3545–3553.

Duderstadt, K.E., Chuang, K., and Berger, J.M. (2011). DNA stretching by bacterial initiators promotes replication origin opening. Nature *478*, 209–213.

Dueber, E.C., Costa, A., Corn, J.E., Bell, S.D., and Berger, J.M. (2011). Molecular determinants of origin discrimination by Orc1 initiators in archaea. Nucleic Acids Res. *39*, 3621–3631.

Dueber, E.L.C., Corn, J.E., Bell, S.D., and Berger, J.M. (2007). Replication origin recognition and deformation by a heterodimeric archaeal Orc1 complex. Science *317*, 1210–1213.

Duggin, I.G., McCallum, S.A., and Bell, S.D. (2008a). Chromosome replication dynamics in the archaeon Sulfolobus acidocaldarius. Proc. Natl. Acad. Sci. USA *105*, 16737–16742.

Duggin, I.G., Wake, R.G., Bell, S.D., and Hill, T.M. (2008b). The replication fork trap and termination of chromosome replication. Mol. Microbiol. *70*, 1323–1333.

Duggin, I.G., Dubarry, N., and Bell, S.D. (2011). Replication termination and chromosome dimer resolution in the archaeon Sulfolobus solfataricus. EMBO J. *30*, 145–153.

Egan, E.S., and Waldor, M.K. (2003). Distinct replication requirements for the two Vibrio cholerae chromosomes. Cell *114*, 521–530.

Egan, E.S., Fogel, M.A., and Waldor, M.K. (2005). Divided genomes: negotiating the cell cycle in prokaryotes with multiple chromosomes. Mol. Microbiol. *56*, 1129–1138.

Erzberger, J.P., Mott, M.L., and Berger, J.M. (2006). Structural basis for ATP-dependent DnaA assembly and replication-origin remodeling. Nat. Struct. Mol. Biol. *13*, 676–683.

Evrin, C., Clarke, P., Zech, J., Lurz, R., Sun, J.C., Uhle, S., Li, H.L., Stillman, B., and Speck, C. (2009). A double-hexameric MCM2-7 complex is loaded onto origin DNA during licensing of eukaryotic DNA replication. Proc. Natl. Acad. Sci. USA *106*, 20240–20245.

French, S.L., Santangelo, T.J., Beyer, A.L., and Reeve, J.N. (2007). Transcription and translation are coupled in Archaea. Mol. Biol. Evol. *24*, 893–895.

Fröls, S., Gordon, P.M.K., Panlilio, M.A., Duggin, I.G., Bell, S.D., Sensen, C.W., and Schleper, C. (2007). Response of the hyperthermophilic archaeon Sulfolobus solfataricus to UV damage. J. Bacteriol. *189*, 8708–8718.

Götz, D., Paytubi, S., Munro, S., Lundgren, M., Bernander, R., and White, M.F. (2007). Responses of hyperthermophilic crenarchaea to UV irradiation. Genome Biol. *8*, R220.

Guo, L., Brügger, K., Liu, C., Shah, S.A., Zheng, H., Zhu, Y., Wang, S., Lillestøl, R.K., Chen, L., Frank, J., et al. (2011). Genome analyses of Icelandic strains of Sulfolobus islandicus, model organisms for genetic and virus-host interaction studies. J. Bacteriol. *193*, 1672–1680.

Heller, R.C., Kang, S., Lam, W.M., Chen, S., Chan, C.S., and Bell, S.P. (2011). Eukaryotic origin-dependent DNA replication in vitro reveals sequential action of DDK and S-CDK kinases. Cell *146*, 80–91.

Kaguni, J.M. (2011). Replication initiation at the Escherichia coli chromosomal origin. Curr. Opin. Chem. Biol. *15*, 606–613.

Katayama, T., Ozaki, S., Keyamura, K., and Fujimitsu, K. (2010). Regulation of the replication cycle: conserved and diverse regulatory systems for DnaA and oriC. Nat. Rev. Microbiol. *8*, 163–170.

Lundgren, M., and Bernander, R. (2007). Genome-wide transcription map of an archaeal cell cycle. Proc. Natl. Acad. Sci. USA *104*, 2939–2944.

Lundgren, M., Andersson, A., Chen, L.M., Nilsson, P., and Bernander, R. (2004). Three replication origins in Sulfolobus species: synchronous initiation of chromosome replication and asynchronous termination. Proc. Natl. Acad. Sci. USA *101*, 7046–7051.

Mott, M.L., and Berger, J.M. (2007). DNA replication initiation: mechanisms and regulation in bacteria. Nat. Rev. Microbiol. *5*, 343–354.

Norais, C., Hawkins, M., Hartman, A.L., Eisen, J.A., Myllykallio, H., and Allers, T. (2007). Genetic and physical mapping of DNA replication origins in Haloferax volcanii. PLoS Genet. *3*, e77.

Ortmann, A.C., Brumfield, S.K., Walther, J., McInnerney, K., Brouns, S.J.J., van de Werken, H.J.G., Bothner, B., Douglas, T., van de Oost, J., and Young, M.J. (2008). Transcriptome analysis of infection of the archaeon Sulfolobus solfataricus with Sulfolobus turreted icosahedral virus. J. Virol. *82*, 4874–4883.

Ozaki, S., Kawakami, H., Nakamura, K., Fujikawa, N., Kagawa, W., Park, S.Y., Yokoyama, S., Kurumizaka, H., and Katayama, T. (2008). A common mechanism for the ATP-DnaA-dependent formation of open complexes at the replication origin. J. Biol. Chem. *283*, 8351–8362.

Park, S.Y., and Asano, M. (2008). The origin recognition complex is dispensable for endoreplication in Drosophila. Proc. Natl. Acad. Sci. USA *105*, 12343–12348.

Randell, J.C.W., Bowers, J.L., Rodríguez, H.K., and Bell, S.P. (2006). Sequential ATP hydrolysis by Cdc6 and ORC directs loading of the Mcm2-7 helicase. Mol. Cell *21*, 29–39.

Remus, D., Beuron, F., Tolun, G., Griffith, J.D., Morris, E.P., and Diffley, J.F.X. (2009). Concerted loading of Mcm2-7 double hexamers around DNA during DNA replication origin licensing. Cell *139*, 719–730.

Robinson, N.P., and Bell, S.D. (2007). Extrachromosomal element capture and the evolution of multiple replication origins in archaeal chromosomes. Proc. Natl. Acad. Sci. USA *104*, 5806–5811.

Robinson, N.P., Dionne, I., Lundgren, M., Marsh, V.L., Bernander, R., and Bell, S.D. (2004). Identification of two origins of replication in the single chromosome of the archaeon Sulfolobus solfataricus. Cell *116*, 25–38.

Robinson, N.P., Blood, K.A., McCallum, S.A., Edwards, P.A.W., and Bell, S.D. (2007). Sister chromatid junctions in the hyperthermophilic archaeon Sulfolobus solfataricus. EMBO J. *26*, 816–824.

Samson, R.Y., Obita, T., Chong, P.L.-G., Williams, R.L., and Bell, S.D. (2011). Molecular and structural basis of ESCRT-III recruitment to membranes during archaeal cell division. Mol. Cell *41*, 186–196.

Scholefield, G., Veening, J.-W., and Murray, H. (2011). DnaA and ORC: more than DNA replication initiators. Trends Cell Biol. *21*, 188–194.

Seki, T., and Diffley, J.F.X. (2000). Stepwise assembly of initiation proteins at budding yeast replication origins in vitro. Proc. Natl. Acad. Sci. USA *97*, 14115–14120.

She, Q., Singh, R.K., Confalonieri, F., Zivanovic, Y., Allard, G., Awayez, M.J., Chan-Weiher, C.C.Y., Clausen, I.G., Curtis, B.A., De Moors, A., et al. (2001). The complete genome of the crenarchaeon Sulfolobus solfataricus P2. Proc. Natl. Acad. Sci. USA *98*, 7835–7840.

Singleton, M.R., Morales, R., Grainge, I., Cook, N., Isupov, M.N., and Wigley, D.B. (2004). Conformational changes induced by nucleotide binding in Cdc6/ORC from Aeropyrum pernix. J. Mol. Biol. *343*, 547–557.

Toro, E., and Shapiro, L. (2010). Bacterial chromosome organization and segregation. Cold Spring Harb. Perspect. Biol. *2*, a000349.

Zhang, C., Guo, L., Deng, L., Wu, Y., Liang, Y., Huang, L., and She, Q. (2010). Revealing the essentiality of multiple archaeal pcna genes using a mutant propagation assay based on an improved knockout method. Microbiology *156*, 3386–3397.

Cell PRESS
Open ACCESS

EXTENDED EXPERIMENTAL PROCEDURES

Gene Knockout Plasmids

A novel gene deletion method recently developed for *Sulfolobus islandicus* REY15A (Deng et al., 2009) was employed to construct gene knockouts of this archaeon for the three *orc1* genes and the other putative replication initiator gene *whip*. This method "Marker cassette Integration and target gene Deletion (MID)" employs three homologous sequence arms, which are target gene arm (G-arm), left sequence arm (L-arm) and right sequence arm (R-arm). The positions of these arms in pLRMG plasmids are illustrated in Figure S5. Primer pairs for each homologous sequence arm were designed to yield a PCR product of ca. 1 kb (Table S2).

The marker cassette of pLRMG plasmids contained *pyrE/F* and *lacS* genes that code for orotate phosphoribosyltransferase, orotidine-5′-monophosphate decarboxylase and β-glycosidase, respectively. Using double markers enabled the transformants obtained on *pyrEF* selection to be verified by a simple X-gal (5-bromo-4-chloro-3-indolyl-β-D- galactopyranoside) screening. These marker genes were obtained by PCR amplification from the *Sulfolobus-E. coli* shuttle plasmid pHZ2lacS with the primer pair of pyrEF+lacS Fwd and pyrEF+lacS Rev (Table S2).

The *E. coli* vector pUC19 was the vector for all pLRMG plasmids construction. The first plasmid pLRMG-orc1-1 was constructed in three steps: First, L-arm and R-arm PCR products were cleaved with SalI + MluI and MluI +EcoRI, respectively and ligated to pUC19 at SalI and EcoRI sites in a triple ligation, yielding pUC-LR. Second, the marker cassette was inserted into the PstI and SalI sites of pUC-LR, giving pUC-LRM. Last, the G-arm was inserted into pUC-LRM at SphI and PstI sites, generating the knockout plasmid pLRMG-orc1-1.

Subsequent construction of other knockout plasmids to be used in this work was based on the pLRMG-orc1-1, following essentially the same strategy. Restriction sites used in pLRMG-orc1-*2* and pLRMG-orc1-3 constructions included SphI and PstI (G-arm); SalI and NcoI (L-arm); and NcoI and BamHI (R-arm). During cloning, a DNA fragment containing the marker cassette and the *orc1*-1 G-arm was cleaved off from pLRMG-orc1-1 with SphI and SalI and the yielded fragment was inserted into the corresponding sites on pUC19, yielding the pUC-M-orc1-1. Then, the *orc1*-1 G-arm was replaced with *orc1*-2 or *orc1*-3, yielding the pUC-M-orc1-2 or the pUC-M-orc1-3. Finally, triple ligations of pUC-M-orc1-2/-orc1-3 with their own L-arm and R-arm yielded pLRMG -orc1-2 and pLRMG-orc1-3, respectively.

Construction of the Plasmid to Inactivate Genome Expression of WhIP Protein Expression

To study if the *whip* gene product could function in origin firing, it was essential to generate a mutant with complete whip gene sequence which lacks WhIP protein expression. For this purpose, we aimed to replace the WT *whip* gene with the mutant gene *whip** which carried three tandem stop codons. The oligonucleotide 5′-ACGCGTTAATGATAA −3′ containing a Mlu I restriction site and three tandem stop codons was inserted between the first and the second codons of whip gene and expression from this whip mutant could only produce a peptide of three amino acids.

Mutant gene *whip** was obtained by SOE-PCR with the four primers listed in Table S2 (under whip*). Then, the SOE-PCR product was inserted into pUC19 at SalI and BamHI sites, yielding pUC-whip*. Marker cassette (cleaved off from pLRMG-orc1-1 with PstI and SalI) was inserted to the pUC-whip* to yield whip* replacement plasmid pUC-M-whip* (Figure S5).

Construction of orc1/whip Mutants of *S. islandicus*

Generation of pLRMG transformants

All pLRMG plasmids were linearized by restriction digestion and 0.9-1μg linearized plasmid DNA was used to transform the genetic host *S. islandicus* E233S by electroporation as described previously (Deng et al., 2009). After incubation at 78°C for 7-10 days, colonies were screened with X-gal. Then, a few blue ones were picked up and inoculated in 6 ml SCVY liquid medium in test tubes and incubated for 3–5 days. The cultures were harvested and genomic DNA extracted. The target gene alleles of these transformants were analyzed by PCR with verifying primer pairs (Table S3).

Isolation of gene deletion mutants by counter-selecting transformants with 5′-FOA.

Once pLRMG-orc1/whip transformants were purified such that the WT allele of the target gene could not be amplified by PCR in the cultures, the transformant cells were diluted and spread onto plates containing uracil and 5′-FOA. Colonies appeared after 7-days incubation. These colonies were first screened with X-gal and a few white colonies were then grown in SCVY medium supplemented with uracil and 5-FOA.Target gene alleles were checked again by PCR and mutant cell lines were confirmed to possess only the deleted target gene allele.

Construction of orc1 double mutants

A second *orc1* gene was to be deleted from a Δorc1 mutant strain to yield double orc1 knockouts. Δ*orc1*-1 was the host for constructing Δ*orc1*-1 Δ*orc1*-2 and Δ*orc1*-1 Δ*orc1*-3 double mutants whereas Δ*orc1*-2 was the host for constructing Δ*orc1*-2 Δ*orc1*-3 mutant and this was done by following single *orc1* mutant construction as described above.

Construction of the Translation-Stop Mutant Gene whip*

The construction of a whip* mutant with three tandem stop codons was a two-steps process (Figure S6). The first step was to select single crossover transformants of the constructed pUC-M-whip*. 1 μg of the plasmid was used to transform the genetic host E233S. Upon entering the cell, homologous recombination between the host genome and the plasmid led to pUC-M-whip* integration either

at Up-seq or Dn-seq. Recombination at Dn-seq was exemplified in Figure S6. After purification, the pUC-M-whip* transformants were subjected to counter selection. Cell lines carrying either the WT or mutant *whip* gene could both grow in the presence of 5-FOA and Uracil. Because a MluI site was introduced into *whip**, mutants carrying *whip** were readily identified by digesting the PCR product of *whip* with MluI.

Analysis of Protein Levels by Western Blot Analysis

Sulfolobus cultures of exponential growth were adjusted to OD_{600} = 0.2 with SCVY. 10 ml of culture was taken and harvested by centrifugation. Cell pellets were resuspended in 0.2 ml H_2O. After adding 0.2 ml 2 × SDS PAGE buffer, the samples were heated at 99°C for 10 min to lyse the cells and denature proteins. Total cellular proteins were then analyzed by SDS/PAGE and Western blot analysis was conducted using antisera against *S. solfataricus* Orc1-1, −2, −3, WhiP protein or PCNA2 or PCNA3 (the latter proteins serving as loading controls). The signals were detected with an enhanced chemiluminescence detection kit (Amersham Biosciences) and recorded with X-ray film.

Neutral-Neutral 2D Gel Electrophoresis

S. islandicus cells were collected by centrifugation and washed twice with TEN buffer (50 mM Tris-Cl, pH 8; 50 mM EDTA, pH 8; 100 mM NaCl). Cell suspensions were then mixed with low melting point agarose and dispensed into Bio-Rad plug molds. Genomic DNA preparation and 2D gel electrophoresis were performed as described previously (Robinson et al., 2004). Specifically, the agarose plugs were digested in NDS buffer (10 mM Tris, pH 9.5; 0.5 M EDTA, pH 8.0; 1% lauroyl sarcosine) containing 1 mg/ml Proteinase K for 48 hr at 37°C. The plugs were then equilibrated in an appropriate restriction buffer before digesting with 500-1000 units of restriction enzyme for approximately 16 hr. See Figure S3 for restriction maps of the *oriC* loci and probe position. A 0.4% agarose gel was poured around the plugs and run for approximately 20 hr at 1 V/cm at 4°C. Lanes containing DNA were excised from the gel, rotated 90°, and incorporated into a 1% agarose gel containing 0.3 μg/ml ethidium bromide. Electrophoresis in the second dimension was carried out at 5 V/cm for 6-7 hr at 4°C. The DNA was depurinated in 0.25 M HCl, then denatured and transferred in 0.5 M NaOH, 10X SSC to Hybond-XL membrane (GE Healthcare) by capillary transfer according to the manufacturer's instructions. ^{32}P-labeled probes (Figure S7; Table S4) were prepared according to the manufacturer's instructions using the NEBlot kit (New England Biolabs). Hybridizations were performed in Church-Gilbert buffer (0.5 M sodium phosphate, 1 mM EDTA, 1% BSA, 7% SDS) at 65°C and washes were performed as described in the Hybond-XL manual. Membranes were exposed to phosphoimager screens which were subsequently scanned on an FLA-5000 phosphoimager (Fujifilm).

Chromatin Immunoprecipitation

Chromatin immunoprecipitation (ChIP) was performed as described in (Robinson et al., 2004) Early logarithmic cultures of *S. islandicus* were crosslinked with 1% formaldehyde for 20 min. After quenching with 125 mM glycine, the cells were pelleted and washed with 1X PBS. The pellets were resuspended in TBS-TT (20 mM Tris, 150 mM NaCl, 0.1% Tween-20, 0.1% Triton X-100, pH 7.5), passed through a French press three times at 20,000 psi, and sonicated using a Diagenode Bioruptor to generate DNA fragments ranging from 200-1000 bp. The extract was then clarified by centrifugation. 10 μg of extract (based on protein concentration) were used in each 100 μl ChIP reaction. Samples were rotated for 2-3 hr with 3 μl of antiserum at 4°C. 25 μl of a 50% slurry of protein A sepharose were then added and the samples were rotated for another hour at 4°C. Each ChIP reaction was then washed five times at room temperature with TBS-TT, once with TBS-TT containing 500 mM NaCl, and once with TBS-TT containing 0.5% Tween-20 and 0.5% Triton X-100. Protein-DNA complexes were eluted from the protein A sepharose in 20 mM Tris, 10 mM EDTA, 0.5% SDS, pH 7.8 at 65°C for 30 min. Crosslinking was reversed and protein was digested by incubating the samples with 10 ng/μl Proteinase K for 6 hr at 65°C followed by 10 hr at 37°C. The samples were extracted with phenol/chloroform/isoamyl alcohol first, then chloroform alone and the DNA was precipitated in 100% ethanol containing 20 μg of glycogen. After washing with 70% ethanol and air-drying, the DNA was resuspended in 50 μl TE buffer. Recovered DNA were either subjected to quantitative PCR or prepared for next generation sequencing on an Illumina Genome Analyzer II (Source Bioscience, UK). Single end sequence reads were mapped to the *S.islandicus* genome using Genious (http://www.geneious.com). The resultant data were exported as .bam files and subsequently analyzed using SeqMonk (http://www.bioinformatics.babraham.ac.uk/projects/seqmonk/). Read counts were quantified in 20 bp windows and was normalized to input DNA.

For qPCR, SYBR detection assays were performed in triplicate using 1 μl of ChIP DNA as template, forward and reverse primers at 125 nM final concentration (Table S5), and Stratagene 2X Brilliant II SYBR Green QPCR Master Mix according to the manufacturer's instructions. Standard curves were prepared in duplicate using ChIP input DNA as template. qPCR reactions and melting curves were performed and analyzed using a Mastercycler ep realplex^2 machine and included analysis software (Eppendorf).

Analytical Ultracentrifugation Analysis of Orc1-1

Orc1-1 (WT and Walker B E147A) proteins were analyzed via sedimentation velocity using a Beckman-Coulter Optima XL-I ultracentrifuge. In each experiment, 450 μl of a 20 μM protein solution were loaded into a sector shaped graphite centrifugation cell. The protein was centrifuged at 50,000 rpm for eight hours while radial scans of absorbance captured the boundary distribution every two minutes until the sample had completely pelleted.

Boundary profiles from sedimentation velocity scans were collected and analyzed using the UltraScan II software suite (Demeler, 2005). Evidence of a highly pure system was observed via model independent enhanced van Holde-Weischet analysis of the data (Demeler et al., 1997) for WT as well as the Walker B mutant. This revealed a tight distribution of the sedimentation coefficient around a value of 3.7 s. Subsequent processing of the complete sedimentation velocity data sets employed 50 iterations of a Genetic Algorithm-Monte Carlo (GA-MC50) model (Brookes and Demeler, 2006). Figure S4 illustrates that the model is able to successfully reproduce the boundary distributions for both species.

Protease Sensitivity Assays

5 μg of purified, recombinant, WT and Walker B mutant Orc1-1 were digested with 0.5 ng/μl trypsin (Roche, sequencing grade) in 100 mM Tris (pH 8.5), 2 mM magnesium acetate, 2 mM ATP, and either 11 μM double-stranded ORB2 or an equivalent volume of water. Samples were removed at 0, 10, 30 min, 1, 3, 5, 7, and 22 hr for time course experiments and at 0 and 22 hr for endpoint digestions. Trypsin digestion was quenched by adding samples to 2.5X protease inhibitor (Roche Complete EDTA-Free Protease Inhibitor Cocktail). An equal volume of 2X SDS-PAGE loading dye was then added to the reactions and the samples were run on 4%–12% Bis-Tris gradient gels before being stained with Coomassie dye. All time course and endpoint experiments were performed a minimum of 5 times each. A representative gel is shown in Figure 7. Mass spectrometry was performed by the Oxford Proteomics Facility.

SUPPLEMENTAL REFERENCES

Brookes, E., and Demeler, B. (2006). Genetic algorithm optimization for obtaining accurate molecular weight distributions from sedimentation velocity experiments. Analytical Ultracentrifugation VIII. Prog. Colloid Polym. Sci. *131*, 78–82.

Demeler, B. (2005). UltraScan: A Comprehensive Data Analysis Software Package for Analytical Ultracentrifugation Experiments. In Modern Analytical Ultracentrifugation: Techniques and Methods, D.J. Scott, S.E. Harding, and A.J. Rowe, eds. (UK: Royal Society of Chemistry), pp. 210–229.

Demeler, B., Saber, H., and Hansen, J.C. (1997). Identification and interpretation of complexity in sedimentation velocity boundaries. Biophys. J. *72*, 397–407.

Peng, N., Xia, Q., Chen, Z., Liang, Y.X., and She, Q. (2009). An upstream activation element exerting differential transcriptional activation on an archaeal promoter. Mol. Microbiol. *74*, 928–939.

Cell PRESS
Open ACCESS

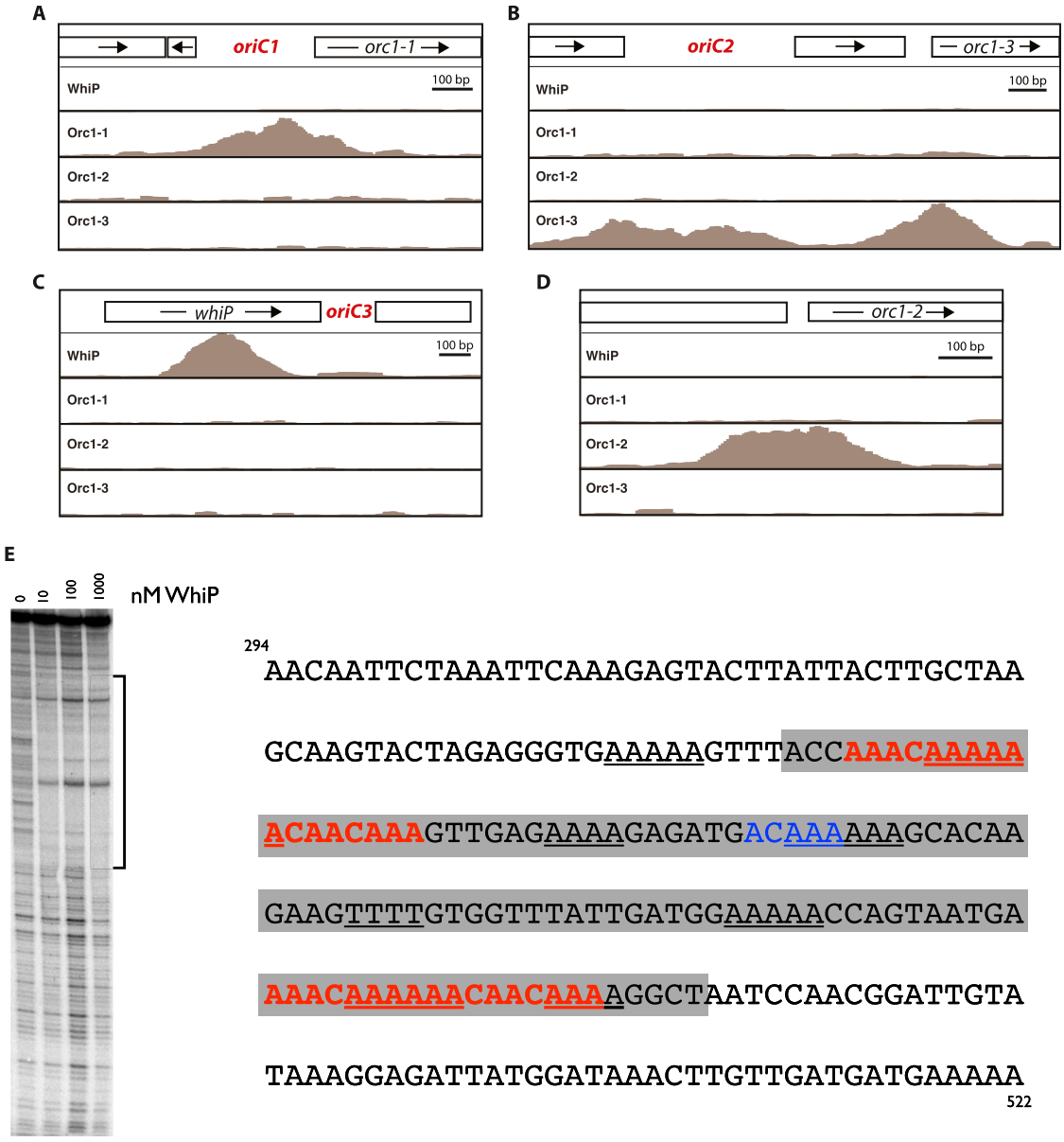

Figure S1. Binding of the Three Orc1/Cdc6 Proteins and WhiP on the Three Origins and the *orc1-2* Promoter Region, Related to Figure 4

(A–D) ChIP Seq profiles of the 4 proteins binding to the indicated loci.

(E) DNaseI footprinting of WhIP binding to sequence repeats within its own ORF. The right panel shows the sequence of the WhiP ORF with a perfect direct repeat indicated in red, runs of four or more A or T residues are indicated by underlining. The gray box indicates the extent of the footprint seen in the left-hand panel.

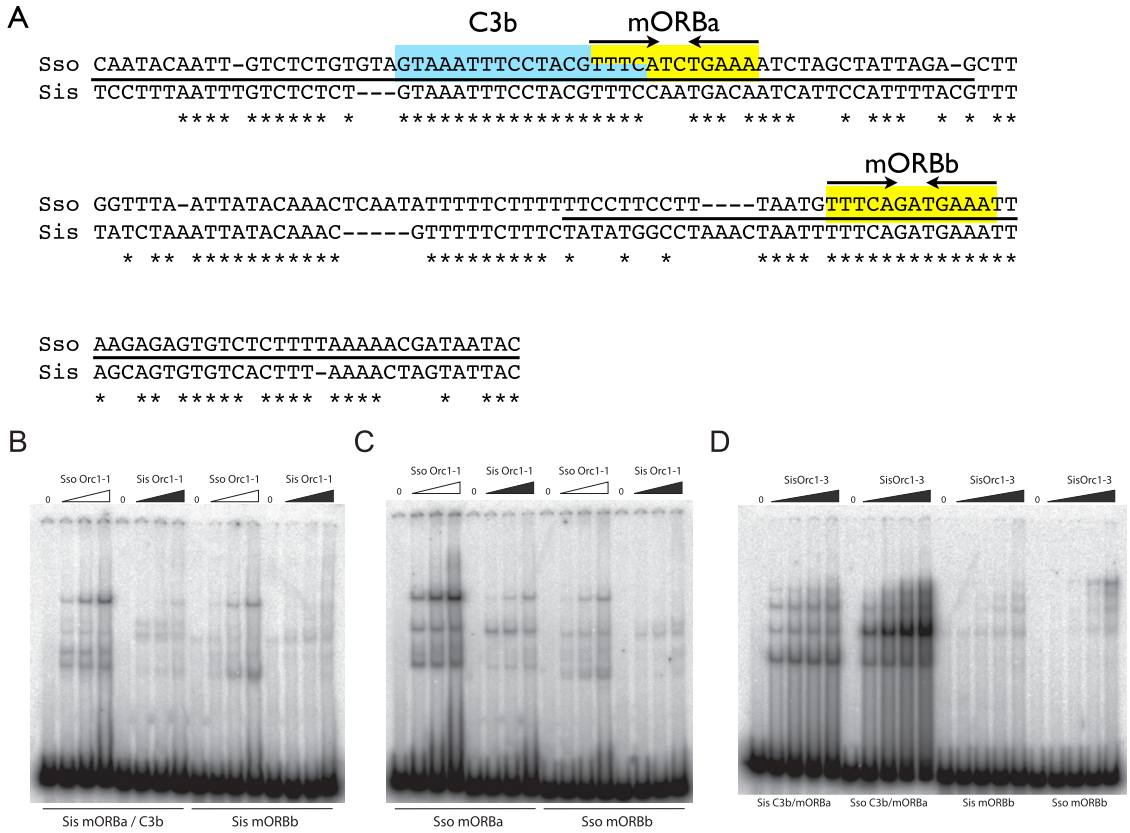

Figure S2. Analysis of Species Specificity of *oriC2* Binding by *S. islandicus* (Sis) and *S. solfataricus* (Sso) Orc1-1 and Orc1-3, Related to Figure 4

Both origin sequence and initiator protein sequence define the differential binding of Orc1-1 to *oriC2* between *S. solfataricus* and *S. islandicus*.

(A) Sequence alignment of the *oriC2* loci from the two species. Asterisks indicate sequence identity. Mapped binding sites for Sso Orc1-1 (mORB elements, yellow) and Orc1-3 (C3b, blue) are highlighted. As can be seen mORBa in *S. islandicus* has four points of sequence divergence from Sso including in the region of dyad symmetry (shown by converging arrows). The underlined regions correspond to the oligonucleotides used in the EMSAs in Figures S2B–S2D.

(B) EMSAs with 0, 0.5, 1 or 2 μM Sso or Sis Orc1-1 on oligonucleotides corresponding to the mORB regions of *S. islandicus oriC2*. While The Sso protein binds readily to these sequences, the cognate Sis protein binds with at least 10-fold lower affinity.

(C) EMSAs with 0, 0.5, 1 or 2 μM Sso or Sis Orc1-1 on oligonucleotides corresponding to the mORB regions of *S. solfataricus oriC2*. Sso Orc1-1 binds to the Sso *oriC2*-derived sequences. Sis Orc1-1 binds with higher affinity to the Sso mORBa sequences than it does to the homologous region of its own species' o*riC2*.

(D) 0, 64, 128, 256, 512 nM Sis Orc1-3 binds to C3b-containing sequences derived from either Sso or Sis *oriC2*.

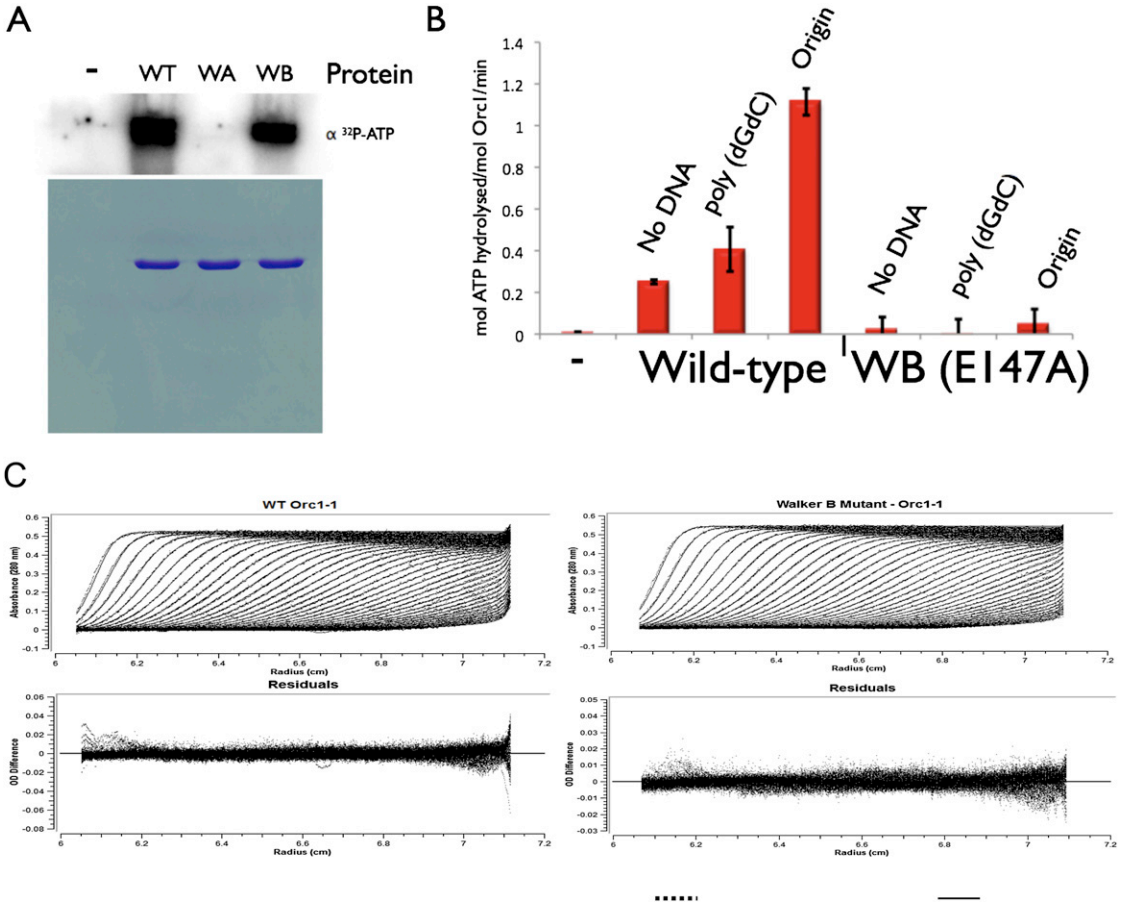

Figure S3. Biochemical Consequences of Walker A and Walker B Mutations of Orc1-1, Related to Figures 5, 6, and 7

(A) 10 μg of refolded WT, Walker A K69A mutant (WA) or Walker (WB) were incubated with 0.375 MBq of α-32P ATP binding. Reactions were split in two and half analyzed by native gel electrophoresis in Tris-glycine, before phosphorimaging of the wet gel (upper panel); the other half was subjected to SDS PAGE (lower panel).

(B) ATPase assays were performed with refolded WT or Walker B (WB) E147A mutant protein. Assays contained no DNA, 20 ng of poly(dGdC) or 20 ng of ORB2 double stranded oligonucleotides.

(C) AUC profiles of WT and Walker B E147A proteins. Upper panels: Sedimentation velocity data (dotted line) and model fit results (solid line) for WT and Walker B Orc1-1. Lower panels: Residuals obtained from 50 iterations of Genetic Algorithm-Monte Carlo analysis of the data set, based on the solution of the hydrodynamic Lamm equation.

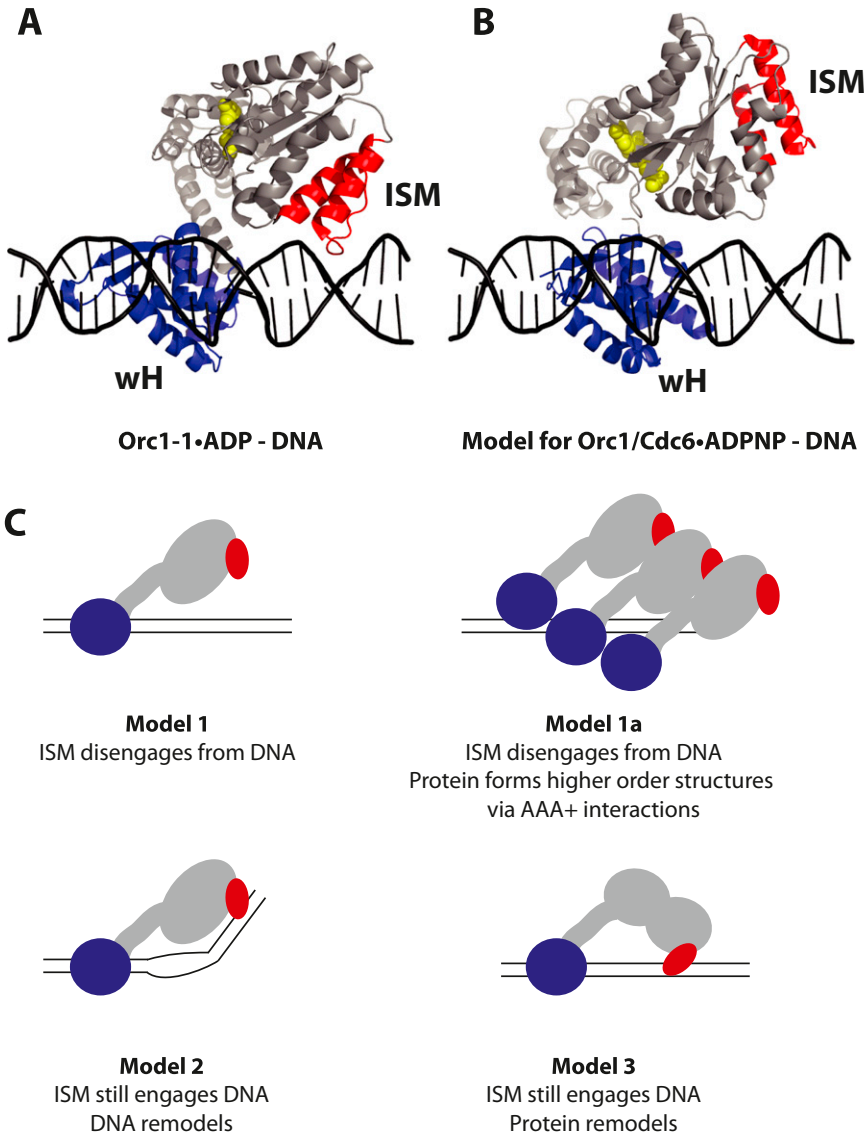

Figure S4. Model for Consequences of ATP Binding by Orc1-1, Related to Figures 5, 6, and 7

(A) Structure of the ADP-bound form of Orc1-1 from *Aeropyrum pernix* bound to DNA (from PDB code 2V1U). The wH domain is shown in blue, the ISM within the AAA+ domain in red and the ADP molecule in yellow. The protein contacts DNA via wH and ISM.

(B) A model of the ADPNP–bound form of the *Aeropyrum* Orc1-2 homolog (Singleton et al., 2004)on DNA. This model was generated by aligning the Orc1-2 protein to the DNA-bound form of Orc1-1 via the wH domain. Color coding is as in part A with ADPNP shown in yellow.

(C) Potential scenarios for the effect of ATP binding by Orc1/Cdc6 protein suggested by the model above. Model 1. ATP binding causes the ISM to disengage from the DNA. An extension of this model is shown in Model 1a where the protein is now able to multimerise into a filament-like structure via the AAA+ domain. This scenario is related to the behavior of DnaA (Erzberger et al., 2006, Duderstadt et al., 2011). In Model 2 both ISM and wH remain bound to DNA in the ATP-bound form, resulting in an alternate conformation of the DNA to that seen in the presence of ADP. Finally, in Model 3 both ISM and wH remain engaged with DNA but the DNA conformation is unaltered but the protein remodels itself relative to the ADP-bound state.

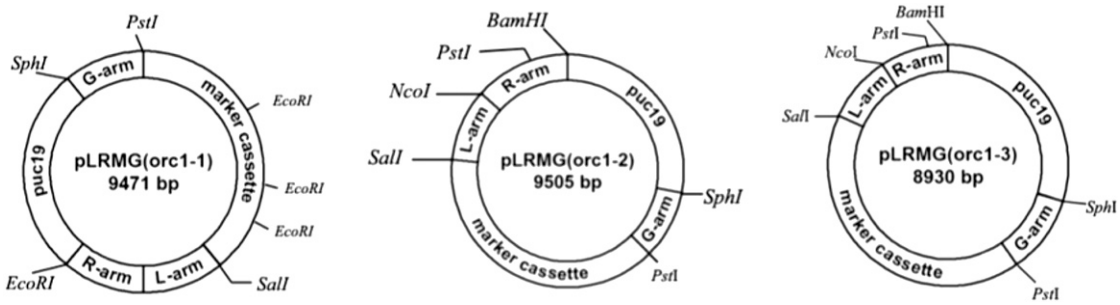

Figure S5. Plasmid Maps for Constructs Used to Generate Knockouts, Related to Figure 1

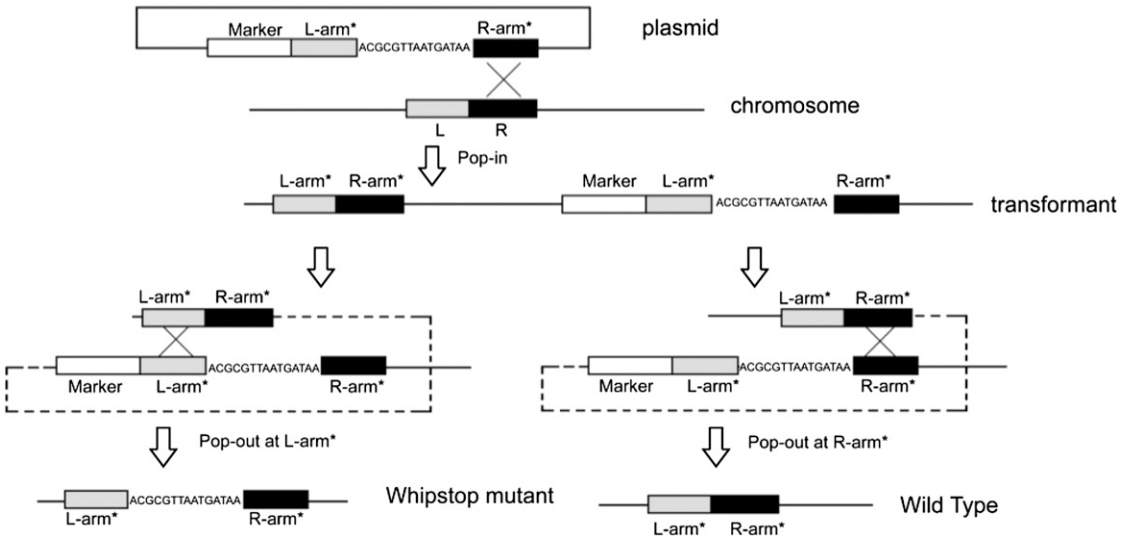

Figure S6. Schematic of the strategy employed to generate the Whip* mutant cell line, Related to Figure 3

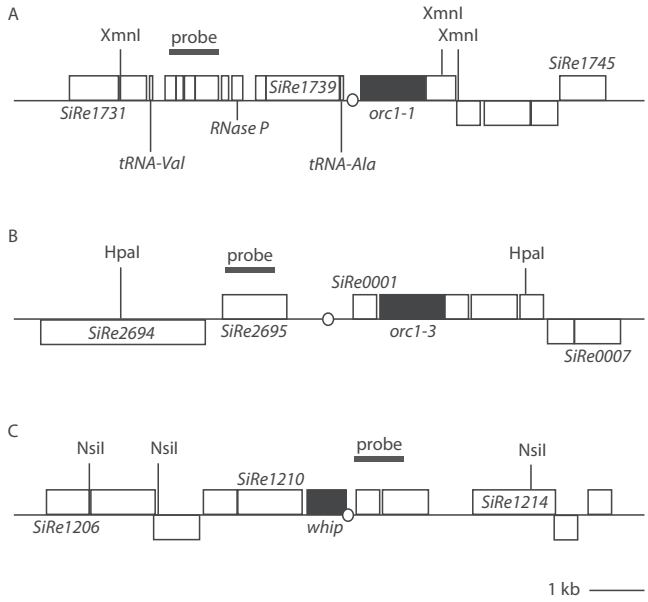

Figure S7. 2D Gel Strategy, Related to Figures 1, 2, 3, 5, and 6

Diagram of the loci encoding (A) *oriC1*, (B) *oriC2* and (C) *oriC3*. Restriction sites and positions of the sequences utilized to generate the radiolabelled probes employed in the 2D gel analyses are indicated. The position of the replication origin in each region is indicated by a circle.